

Ligand-Induced Tuning of the Oxidase Activity of μ -Hydroxidodimanganese(III) Complexes Using 3,5-Di-*tert*-butylcatechol as the Substrate: Isolation and Characterization of Products Involving an Oxidized Dioxolene Moiety

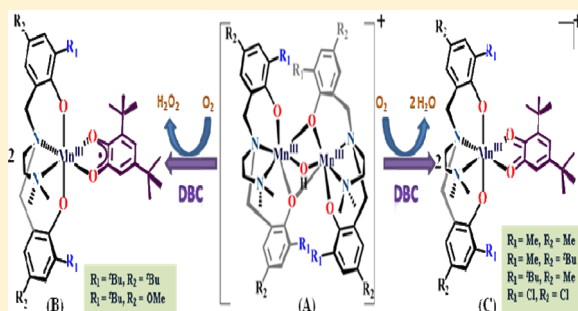
Dhrubajyoti Mondal,[†] Sanchita Kundu,[†] Mithun Chandra Majee,[†] Atanu Rana,[†] Akira Endo,[‡] and Muktimoy Chaudhury^{*,†}

[†]Department of Inorganic Chemistry, Indian Association for the Cultivation of Science, Jadavpur, Kolkata 700 032, India

[‡]Department of Materials and Life Sciences, Faculty of Science and Technology, Sophia University, 7-1 Kioi-cho, Chiyoda-ku, Tokyo 102-8554, Japan

Supporting Information

ABSTRACT: Oxidase activities of a μ -hydroxidodimanganese(III) system involving a series of tetradentate capping ligands $H_2L^{R_1,R_2}$ with a pair of phenolate arms have been investigated in the presence of 3,5-di-*tert*-butylcatechol (H_2 DBC) as a coligand cum-reductant. The reaction follows two distinctly different paths, decided by the substituent combinations (R_1 and R_2) present in the capping ligand. With the ligands $H_2L^{t-Bu,t-Bu}$ and $H_2L^{t-Bu,OMe}$, the products obtained are semiquinonato compounds $[Mn^{III}(L^{t-Bu,t-Bu})(DBSQ)] \cdot 2CH_3OH$ (1) and $[Mn^{III}(L^{t-Bu,OMe})(DBSQ)] \cdot CH_3OH$ (2), respectively. In the process, molecular oxygen is reduced by two electrons to generate H_2O_2 in the solution, as confirmed by iodometric detection. With the rest of the ligands, viz., $H_2L^{Me,Me}$, $H_2L^{t-Bu,Me}$, $H_2L^{Me,t-Bu}$, and $H_2L^{Cl,Cl}$, the products initially obtained are believed to be highly reactive quinonato compounds $[Mn^{III}(L^{R_1,R_2})(DBQ)]^+$, which undergo a domino reaction with the solvent methanol to generate products of composition $[Mn^{III}(L^{R_1,R_2})(BMOD)]$ (3–6) involving a nonplanar dioxolene moiety, viz., 3,5-di-*tert*-butyl-3-methoxy-6-oxocyclohexa-1,4-dienolate (BMOD[−]). This novel dioxolene derivative is formed by a Michael-type nucleophilic 1,4-addition reaction of the methoxy group to the coordinated quinone in $[Mn^{III}(L^{R_1,R_2})(DBQ)]^+$. During this reaction, molecular oxygen is reduced by four electrons to generate water. The products have been characterized by single-crystal X-ray diffraction analysis as well as by spectroscopic methods and magnetic measurements. Density functional theory calculations have been made to address the observed influence of the secondary coordination sphere in tuning the two-electron versus four-electron reduction of dioxygen. The semiquinone form of the dioxolene moiety is stabilized in compounds 1 and 2 because of extended electron delocalization via participation of the appropriate metal orbital(s).



INTRODUCTION

Activation of dioxygen (O_2) by transition-metal ions plays a pivotal role in many biological and industrial oxidation processes.¹ Oxidases are a group of ubiquitous metalloenzymes that use such activated O_2 as an electron acceptor to carry out the proton-assisted selective oxidation of organic substrates.² In the process, oxygen is often reduced by four electrons to generate water or by two electrons to generate hydrogen peroxide (H_2O_2) depending upon the types of the metal-ion activators involved.³ The former type of oxidation plays an essential role in the sustenance of life processes (aerobic respiration).⁴ Industrially, also oxidation of this type is harnessed quite efficiently in the development of new fuel cell technology.⁵ A two-electron O_2 reduction, on the other hand, generates H_2O_2 , a versatile oxidizing agent ideal for doing green chemistry.⁶ Various factors have been reported in the

literature that control the two-electron versus four-electron reduction of O_2 catalyzed by metal-ion activators. These include their optimized coordination geometry, steric factors, and donor-atom combination and the net charge provided by the primary coordination sphere that surrounds the metal center.⁷

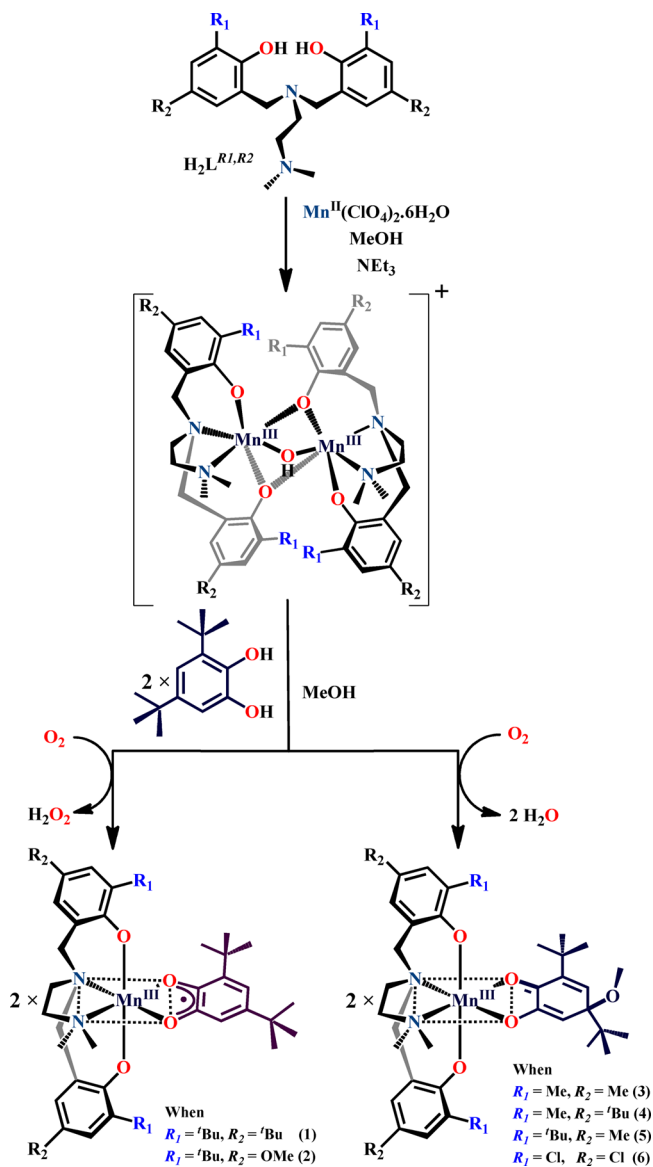
Nature uses various transition-metal ions for the activation of O_2 , which is otherwise kinetically inert.⁸ Both iron and copper have shown their preference for catalyzing those oxidation reactions.^{9,10} Manganese also exhibits rich O_2 chemistry in both biological and synthetic systems. Its useful redox properties have been utilized by nature in accumulating manganese in a host of redox-active metalloenzymes.¹¹ A number of key

Received: January 17, 2017

reactions involving O_2 and its reduced forms (water, peroxide, and superoxide) are promoted by many manganese-dependent enzymes that include lipoxygenase,¹² ribonucleotide reductase,¹³ superoxide dismutase,¹⁴ catalases,¹⁵ and the oxygen-evolving complex of photosystem II.¹⁶ A large number of bioinspired model manganese complexes are known to mimic the structure and/or reactivity of the aforementioned enzymes.^{17,18}

Herein we report the oxidase activity of a new manganese(III) system involving a family of facially coordinating N_2O_2 ligands with a pair of appended phenolate arms ($H_2L^{R_1,R_2}$, shown in Scheme 1) that combine with $[Mn(ClO_4)_2] \cdot 6H_2O$ in

Scheme 1. Synthesis Protocol for Complexes 1–6



the mandatory presence of 3,5-di-*tert*-butylcatechol (H_2DBC)¹⁹ as a reductant to generate either a semiquinonato or a quinonato product (1–6) due to a two- or four-electron reduction of O_2 , respectively. The products have been characterized by X-ray diffraction analysis as well as spectroscopic methods. Density functional theory (DFT) calculations have been made to identify the causative factor(s) that tune the changeover of the stoichiometry of O_2 reduction

between two and four electrons during the course of these oxidase actions.

EXPERIMENTAL SECTION

Materials. All reactions were carried out in an aerobic environment unless stated otherwise, with chemicals available from commercial sources and used as received. The solvents were of reagent grade and were dried by a standard procedure²⁰ and distilled under nitrogen prior to their use. The tetradentate bisphenol N_2O_2 ligands $H_2L^{R_1,R_2}$ (summarized in Scheme 1) were prepared following a modified procedure of a reported method.²¹

Synthesis of Ligands. A modified procedure for the synthesis of *N,N*-bis(2-hydroxy-3,5-di-*tert*-butylbenzyl)-*N,N'*-dimethylethylenediamine ($H_2L^{t-Bu,t-Bu}$) is described here as a prototype. To a solution of 2,4-di-*tert*-butylphenol (4.12 g, 20 mmol) in methanol (30 mL) were added *N,N*-dimethylethylenediamine (0.88 g, 10 mmol) and paraformaldehyde (60 mg, 20 mmol). The resulting solution was refluxed for 15 h. It was then cooled to room temperature and rotary-evaporated to ca. 10 mL volume. The resulting white precipitate was filtered off, washed with 20 mL of cold methanol, and recrystallized from a dichloromethane/methanol (1:1, v/v) mixture. Yield: 3.7 g (70%). Mp: 131 °C. Anal. Calcd for $C_{34}H_{56}N_2O_2$: C, 77.75; H, 10.94; N, 5.31. Found: C, 77.84; H, 10.80; N, 5.30. ¹H NMR (400 MHz, $CDCl_3$, δ /ppm): 1.27 (s, 18H, CH_3 of *t*-Bu), 1.39 (s, 18H, CH_3 of *t*-Bu), 2.32 (s, 6H, CH_3 of $N(CH_3)_2$), 2.58 (m, $J = 7.0$ Hz, 4H, $(Me)_2NCH_2CH_2-$), 3.61 (s, 4H, $ArCH_2$), 6.88 (d, $^4J_{HH} = 2.0$ Hz, 2H, aryl), 7.20 (d, $^4J_{HH} = 2.0$ Hz, 2H, aryl), 9.81 (s, 2H, phenolic OH). UV-vis [CH_3CN ; λ_{max} nm (ϵ , $L mol^{-1} cm^{-1}$): 280 (5600), 228 (13700). ESI-MS (positive) in CH_3CN : m/z 525.50 (100%, $M + H^+$). A representative ¹H NMR spectrum of the ligand $H_2L^{t-Bu,t-Bu}$ is displayed in Figure S1 (in the Supporting Information). Detailed characterization data of the remaining ligands are also summarized in the Supporting Information.

Preparation of Complexes. **Safety Note!** Perchlorate salts of metal complexes are potentially explosive and should be handled only in small quantities with sufficient care.²²

$[Mn^{III}(L^{t-Bu,t-Bu})(DBSQ)] \cdot 2CH_3OH$ (1).¹⁹ To a stirred solution of $H_2L^{t-Bu,t-Bu}$ (131 mg, 0.25 mmol) in methanol (25 mL) was added Et_3N (0.5 mmol), followed by $[Mn(ClO_4)_2 \cdot 6H_2O]$ (90 mg, 0.25 mmol), and the solution was refluxed for 1 h, during which a dark-brown solution was obtained. It was cooled to room temperature, and 3,5-di-*tert*-butylcatechol (55 mg, 0.25 mmol) was added in small portions over a period of 1 h with constant stirring. The precipitated dark-brown microcrystalline solid was isolated by filtration, dried in air, and finally recrystallized from a dichloromethane/methanol (1:1, v/v) mixture. Yield: 104 mg (50%). Some of these crystals were of diffraction quality and were used directly for X-ray crystal structure analysis. Anal. Calcd for $C_{50}H_{82}N_2O_6Mn$: C, 69.66; H, 9.59; N, 3.25. Found: C, 69.61; H, 9.39; N, 3.32. FT-IR bands (KBr pellet, cm^{-1}): 2956 vs, 2904 s, 2856 m, 1480 s, 1465 vs, 1442 vs, 1409 m, 1359 m, 1259 s, 1244 s, 1203 m, 835 m, 557 m. UV-vis [CH_2Cl_2 ; λ_{max} nm (ϵ , $L mol^{-1} cm^{-1}$): 292 (20000), 370 (7900), 488 (4200), 700 (1350). μ_{eff} (solid, 25 °C): 3.94 μ_B .

$[Mn^{III}(L^{t-Bu,OMe})(DBSQ)] \cdot CH_3OH$ (2). This compound was prepared following essentially the same procedure as that described for compound 1 using the ligand $H_2L^{t-Bu,OMe}$. The X-ray-quality crystals of this compound were grown from a methanol solution at 4 °C. Yield: 45%. Anal. Calcd for $C_{43}H_{66}N_2O_7Mn$: C, 66.39; H, 8.55; N, 3.60. Found: C, 66.52; H, 8.49; N, 3.67. FT-IR bands (KBr pellet, cm^{-1}): 2954 s, 2869 s, 1490 s, 1461 vs, 1427 s, 1357 m, 1242 s, 1205 s, 1062 m, 821 m, 811 m. UV-vis [CH_2Cl_2 ; λ_{max} nm (ϵ , $L mol^{-1} cm^{-1}$): 303 (24200), 377 (7400), 495 (4000), 724 (1550). μ_{eff} (solid, 25 °C): 3.89 μ_B .

$[Mn^{III}(L^{Me,Me})(BMOD)] \cdot 2CH_3OH$ (3).¹⁹ Method A. This compound was prepared following essentially the same procedure as that described for compound 1 using the ligand $H_2L^{Me,Me}$. X-ray-quality crystals were grown from a methanol solution at 4 °C. Yield: 47%. Anal. Calcd for $C_{39}H_{61}N_2O_7Mn$: C, 64.62; H, 8.48; N, 3.86. Found: C, 64.38; H, 8.61; N, 3.90. FT-IR bands (KBr pellet, cm^{-1}): 2956 m,

2908 m, 1606 vs, 1473 vs, 1427 s, 1361 m, 1247 s, 1161 m, 1070 m, 956 m, 823 m, 609 m, 557 m. UV–vis [CH_2Cl_2 ; λ_{max} nm (ϵ , $\text{L mol}^{-1} \text{cm}^{-1}$): 281 (18500), 373 (6650), 505 (2900), 661 (660). μ_{eff} (solid, 25 °C): 4.54 μ_{B}

$[\text{Mn}^{\text{III}}(\text{L}^{\text{Me},t\text{-Bu}})(\text{BMOD})]\cdot\text{CH}_3\text{OH}$ (**4**). This compound was prepared following essentially the same procedure as that described for compound **1** using the ligand $\text{H}_2\text{L}^{\text{Me},t\text{-Bu}}$ instead of $\text{H}_2\text{L}^{\text{t-Bu},t\text{-Bu}}$. The X-ray-quality crystals were grown from a methanol solution at 4 °C. Yield: 50%. Anal. Calcd for $\text{C}_{44}\text{H}_{69}\text{N}_2\text{O}_6\text{Mn}$: C, 68.02; H, 8.95; N, 3.61. Found: C, 67.87; H, 9.07; N, 3.66. FT-IR bands (KBr pellet, cm^{-1}): 2958 s, 1606 vs, 1475 vs, 1361 m, 1267 m, 1218 m, 1072 m, 950 m, 835 m, 605 m, 549 m. UV–vis [CH_2Cl_2 ; λ_{max} nm (ϵ , $\text{L mol}^{-1} \text{cm}^{-1}$): 277 (17400), 374 (5700), 509 (2300). μ_{eff} (solid, 25 °C): 4.88 μ_{B}

$[\text{Mn}^{\text{III}}(\text{L}^{\text{t-Bu},\text{Me}})(\text{BMOD})]$ (**5**). This compound was prepared following essentially the same procedure as that described for compound **1** using the ligand $\text{H}_2\text{L}^{\text{t-Bu},\text{Me}}$ instead of $\text{H}_2\text{L}^{\text{t-Bu},t\text{-Bu}}$. The X-ray-quality crystals were grown from a methanol solution at 4 °C. Yield: 43%. Anal. Calcd for $\text{C}_{43}\text{H}_{65}\text{N}_2\text{O}_5\text{Mn}$: C, 69.33; H, 8.79; N, 3.76. Found: C, 69.03; H, 8.94; N, 3.77. FT-IR bands (KBr pellet, cm^{-1}): 2954 vs, 2908 s, 1604 vs, 1463 vs, 1442 s, 1251 m, 1157 m, 1078 m, 825 m, 609 m, 555 m. UV–vis [CH_2Cl_2 ; λ_{max} nm (ϵ , $\text{L mol}^{-1} \text{cm}^{-1}$): 289 (14900), 375 (5650), 511 (1550). μ_{eff} (solid, 25 °C): 4.55 μ_{B}

$[\text{Mn}^{\text{III}}(\text{L}^{\text{Cl},\text{Cl}})(\text{BMOD})]\cdot\text{H}_2\text{O}$ (**6**). This complex was also prepared in a manner similar to that for **1** using the ligand $\text{H}_2\text{L}^{\text{Cl},\text{Cl}}$. The X-ray-quality crystals were grown from a methanol solution at 4 °C. Yield: 40%. Anal. Calcd for $\text{C}_{33}\text{H}_{43}\text{N}_2\text{O}_6\text{Cl}_4\text{Mn}$: C, 52.12; H, 5.70; N, 3.68. Found: C, 52.52; H, 5.64; N, 3.72. FT-IR bands (KBr pellet, cm^{-1}): 2960 vs, 1606 s, 1458 vs, 1303 s, 1245 m, 1070 m, 865 m, 767 m, 757 m, 597 m. UV–vis [CH_2Cl_2 ; λ_{max} nm (ϵ , $\text{L mol}^{-1} \text{cm}^{-1}$): 287 (13000), 376 (4150), 523 (1080). μ_{eff} (solid, 25 °C): 4.79 μ_{B}

$[(\text{L}^{\text{Me},\text{Me}}\text{Mn}^{\text{III}})_2(\mu\text{-OMe})]\text{BPh}_4$ (**7**). To a stirred solution of $\text{H}_2\text{L}^{\text{Me},\text{Me}}$ (131 mg, 0.25 mmol) in methanol (25 mL) was added Et_3N (0.5 mmol), followed by $[\text{Mn}(\text{ClO}_4)_2\cdot 6\text{H}_2\text{O}]$ (90 mg, 0.25 mmol), and the solution was refluxed for 1 h, during which a dark-brown solution was obtained and then cooled to room temperature. To this was added a solution of sodium tetraphenylborate (86 mg, 0.25 mmol) in methanol (5 mL) under constant stirring. The resulting solution was stirred for another 15 min and then filtered. The filtrate was kept in a refrigerator at 4 °C. A very thin needle-shaped microcrystalline compound was grown from this solution after ca. 2 days. A few of these crystals were barely of diffraction-quality and were used directly for X-ray data collection. Yield: 240 mg (72%). Anal. Calcd for $\text{C}_{69}\text{H}_{83}\text{N}_4\text{O}_5\text{BMn}_2$: C, 70.89; H, 7.16; N, 4.79. Found: C, 70.68; H, 6.99; N, 4.75. FT-IR bands (KBr pellet, cm^{-1}): 2920 m, 2869 s, 1471 vs, 1249 s, 1161 m, 832 m, 821 m, 734 m, 705 m, 611 m. ESI-MS (positive) in CH_3CN : 835.62 $[(\text{L}^{\text{Me},\text{Me}}\text{Mn}^{\text{III}})_2(\mu\text{-OH})]^+$, 849.63 $[(\text{L}^{\text{Me},\text{Me}}\text{Mn}^{\text{III}})_2(\mu\text{-OMe})]^+$, 409.32 $[\text{L}^{\text{Me},\text{Me}}\text{Mn}^{\text{III}}]^+$.

$[(\text{L}^{\text{Me},t\text{-Bu}}\text{Mn}^{\text{III}})_2(\mu\text{-OMe})]\text{BPh}_4$ (**8**). This compound was prepared following essentially the same procedure as that described for compound **7** using the ligand $\text{H}_2\text{L}^{\text{Me},t\text{-Bu}}$. Yield: 68%. Anal. Calcd for $\text{C}_{81}\text{H}_{107}\text{N}_4\text{O}_5\text{BMn}_2$: C, 72.74; H, 8.06; N, 4.19. Found: C, 72.61; H, 7.87; N, 4.23. FT-IR bands (KBr pellet, cm^{-1}): 2960 vs, 2923 s, 1479 vs, 1263 m, 1217 s, 837 m, 734 m, 705 m, 613 m. ESI-MS (positive) in CH_3CN : 1003.24 $[(\text{L}^{\text{Me},t\text{-Bu}}\text{Mn}^{\text{III}})_2(\mu\text{-OH})]^+$, 511.08 $[\text{L}^{\text{Me},t\text{-Bu}}\text{Mn}^{\text{III}}(\text{OH})]^+$ + H^+ , 493.02 $[\text{L}^{\text{Me},t\text{-Bu}}\text{Mn}^{\text{III}}]^+$.

Compounds **3–6** have been also synthesized following an alternative procedure (method B). Details of this procedure have been described below for compound **3** as a representative example.

Compound 3. Method B. To a stirred solution of $\text{H}_2\text{L}^{\text{Me},\text{Me}}$ (89 mg, 0.25 mmol) in methanol (25 mL) was added Et_3N (0.5 mmol), followed by $[\text{Mn}(\text{ClO}_4)_2\cdot 6\text{H}_2\text{O}]$ (90 mg, 0.25 mmol), and the solution was refluxed for 1 h in an anaerobic environment, during which a dark-brown solution was obtained and then cooled to room temperature. 3,5-Di-*tert*-butyl-*o*-benzoquinone (55 mg, 0.25 mmol) was then added in small portions over a period of 1 h with constant stirring. The resulting solution was filtered over a Celite bed; the filtrate volume was reduced to about 15 mL by rotary evaporation and then kept in a refrigerator at 4 °C. The product was obtained as a brown crystalline solid within 2–3 days. Yield: 100 mg (56%). Some

of these crystals were of diffraction-quality and were used directly for X-ray crystal structure analysis. Anal. Calcd for $\text{C}_{39}\text{H}_{61}\text{N}_2\text{O}_7\text{Mn}$: C, 64.62; H, 8.48; N, 3.86. Found: C, 64.58; H, 8.19; N, 3.80. This compound shows an overlapping IR spectrum with compound **3**, prepared by method A.

Physical Measurements. IR spectroscopic measurements were made on samples pressed into KBr pellets using a Shimadzu 8400S Fourier transform infrared (FT-IR) spectrometer, while for UV–vis spectral measurements, a PerkinElmer Lambda 950 UV–vis–near-IR spectrophotometer was employed. Elemental analyses (for C, H, and N) were performed at IACS on a PerkinElmer model 2400 series II CHNS analyzer. The electrospray ionization mass spectrometry (ESI-MS) spectra in positive-ion mode were measured on a Micromass QTOF model YA 263 mass spectrometer. The ^1H NMR spectra were recorded on a Bruker model Avance DPX-400 spectrometer using tetramethylsilane as the internal reference. Magnetic moments at room temperature were measured on a Gouy balance (Sherwood Scientific, Cambridge, U.K.). Diamagnetic contributions were estimated using Pascal's constants.

Cyclic voltammetry in dichloroethane (DCE) was recorded on a BAS model 100 B/W electrochemical workstation using a glassy carbon working electrode and a platinum wire counter electrode. Silver/silver chloride (Ag/AgCl) was used for the reference electrode and ferrocene/ferrocenium as the internal standard. Solutions were ~1.0 mM in samples and contained 0.1 M tetrabutylammonium perchlorate (TBAP) as the supporting electrolyte.

Detection of Hydrogen Peroxide (H_2O_2). Accumulation of H_2O_2 in the reaction mixture during the synthesis of complexes **1–6** in an aerobic environment was monitored spectrophotometrically by following the development of the characteristic band at 353 nm for I_3^- ($\epsilon = 26000 \text{ L mol}^{-1} \text{cm}^{-1}$), generated because of oxidation of I^- by H_2O_2 .^{23,24} In a typical experiment, the ligand $\text{H}_2\text{L}^{\text{t-Bu},t\text{-Bu}}$ (32 mg, 0.06 mmol) was added to a solution of $\text{Mn}(\text{ClO}_4)_2\cdot 6\text{H}_2\text{O}$ (45 mg, 0.06 mmol) in methanol (15 mL), followed by triethylamine (NET_3 ; 12 mg, 0.12 mmol). The solution was refluxed for 1 h and then cooled to room temperature. To this cold solution was added $\text{H}_2\text{DBC}^{19}$ (55 mg, 0.25 mmol), and the resulting solution was stirred for ca. 15 min to generate the semiquinonato compound **1**. The solution was rotary-evaporated to ca. 5 mL volume. Dichloromethane (20 mL) and an equal volume of water were added subsequently in order to extract compound **1** into the dichloromethane layer, leaving H_2O_2 in water. The process was repeated three times. The aqueous layer was acidified with H_2SO_4 (ca. 10^{-2} M) to pH 2 to stop further oxidation, and 1 mL of a 10% aqueous solution of KI and 3 drops of a 3% solution of ammonium molybdate were added. In the presence of H_2O_2 , iodide is quantitatively oxidized to liberate iodine, which is stabilized as a I_3^- ion in the solution. The rate of this oxidation is usually quite slow but becomes almost instantaneous after the addition of a catalytic amount of molybdate solution.²⁵ The growth of a band at 353 nm due to the formation of I_3^- was monitored. Because iodide ion in an acidic solution is oxidized by aerial O_2 , blank experiments were also done to check the experimental data.

DFT Calculations. All calculations were performed in the Inorganic Chemistry HPC cluster at IACS. The geometries were optimized using the 6-31g* basis set on Mn, C, N, O, and H atoms using Gaussian 03, version C03, using the B3LYP functional and spin-unrestricted formalism.^{26–29} The fully optimized structures were confirmed by doing the frequency calculations to show that no imaginary modes were present for all of these compounds. The final energy calculations were performed using the 6-311+g* basis set on all atoms.

X-ray Crystallography. Suitable crystals of **1** (dark-brown block, $0.23 \times 0.21 \times 0.15 \text{ mm}^3$), **2** (dark-brown block, $0.15 \times 0.15 \times 0.12 \text{ mm}^3$), **3** (brown block, $0.24 \times 0.20 \times 0.15 \text{ mm}^3$), **4** (brown block, $0.25 \times 0.18 \times 0.15 \text{ mm}^3$), **5** (brown block, $0.15 \times 0.20 \times 0.14 \text{ mm}^3$), **6** (brown block, $0.18 \times 0.15 \times 0.12 \text{ mm}^3$), **7** (brown needle, $0.15 \times 0.06 \times 0.05 \text{ mm}^3$), and **8** (brown needle, $0.16 \times 0.08 \times 0.06 \text{ mm}^3$) were mounted on glass fibers coated with perfluoropolyether oil before mounting. Intensity data for the aligned crystals were measured by employing a Bruker SMART APEX II CCD diffractometer equipped

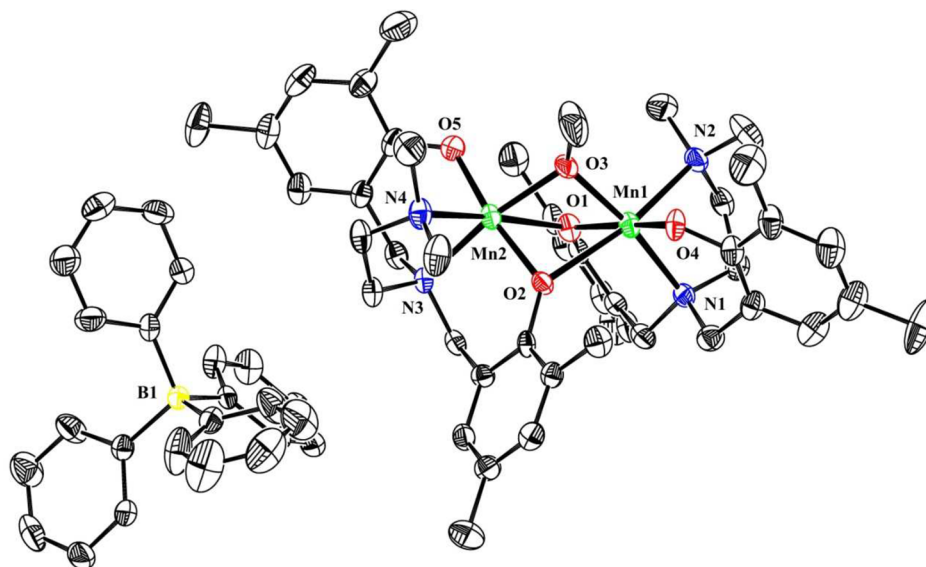


Figure 1. Molecular structure and atom-labeling scheme for complex 7 with thermal ellipsoids drawn at the 30% probability level. H atoms have been omitted for clarity.

with a monochromatized Mo $K\alpha$ radiation ($\lambda = 0.71073 \text{ \AA}$) source at 293(2) K except for compounds 1 and 4, which were measured at 150(2) K. No crystal decay was observed during data collection. In all cases, absorption corrections based on multiscans using the *SADABS* software³⁰ were applied. The structures were solved by direct methods³¹ and refined on F^2 by a full-matrix least-squares procedure based on all data minimizing $wR = [\sum[w(F_o^2 - F_c^2)^2]/\sum(F_o^2)^2]^{1/2}$, $R = \sum||F_o| - |F_c||/\sum|F_o|$, and $S = [\sum[w(F_o^2 - F_c^2)^2]/(n - p)]^{1/2}$. *SHELXL-2013* was used for both structure solutions and refinements.³² A summary of the relevant crystallographic data and the final refinement details is given in [Table S1](#).

All non-H atoms were refined anisotropically. The H atoms were calculated and isotropically fixed in the final refinement [$d(\text{C-H}) = 0.95 \text{ \AA}$, with the isotropic thermal parameter of $U_{\text{iso}}(\text{H}) = 1.2U_{\text{iso}}(\text{C})$]. The *SMART* and *SAINTE* software packages³³ were used for data collection and reduction, respectively. Crystallographic diagrams were drawn using the *Diamond* software package.³⁴ The CCDC reference numbers for the crystal structures of complexes 1–7 are 1548156–1548162.

RESULTS AND DISCUSSION

Synthesis. A new family of facially coordinating tetradentate diphenol ligands ($\text{H}_2\text{L}^{\text{R}_1, \text{R}_2}$, shown in [Scheme 1](#)) have been synthesized. These ligands in an aerobic environment react with $\text{Mn}(\text{ClO}_4)_2 \cdot 6\text{H}_2\text{O}$ in methanol in the presence of an added base (NEt_3) and H_2DBC as the coligand. The isolated products 1–6 are of two different types, each involving an oxidized form of the dioxolene coligand, and appear to be controlled by the substituent combinations (R_1 and R_2) present in the capping ligand ($\text{H}_2\text{L}^{\text{R}_1, \text{R}_2}$) framework. Thus, in compounds 1 and 2, in which the capping ligands have the substitution combinations of *t*-Bu, *t*-Bu (in 1) and *t*-Bu, OMe (in 2), the added coligand is oxidized to the 3,5-*di-tert*-butylsemiquinonato anion (DBSQ^-) and remains coordinated to the Mn^{III} center. In the rest of the products (3–6), oxidation of the coligand proceeds further, leading to the generation of a new monoanionic ligand, viz., 3,5-*di-tert*-butyl-3-methoxy-6-oxocyclohexa-1,4-dienolate (BMOD^-) in which the aromaticity of the precursor DBC^{2-} coligand is lost. A methoxy group from the solvent methanol is accommodated in the oxidized dioxolene ring, forming a σ -bond with the lone sp^3 -hybridized C center in the ring ([Scheme 1](#)).

In order to have a better understanding of these complicated redox reactions, we decided to reevaluate the whole synthetic procedure by carrying out the reactions in two consecutive steps. In the initial step, the capping ligand $\text{H}_2\text{L}^{\text{R}_1, \text{R}_2}$ in refluxing methanol was allowed to react with $\text{Mn}(\text{ClO}_4)_2 \cdot 6\text{H}_2\text{O}$ in an aerobic environment in the presence of Et_3N . The products in all cases, unfortunately, were intractable solids. ESI-MS spectra of these solids indicate that these are all cationic complexes involving the $[(\text{L}^{\text{R}_1, \text{R}_2}\text{Mn}^{\text{III}})_2(\mu\text{-OH})]^+$ molecular ion. However, using a bulky anion, viz., tetraphenylborate, in the reaction mixture, we became successful to isolate the OMe-bridged binuclear Mn^{III} complexes 7 and 8 as crystalline solids when $\text{H}_2\text{L}^{\text{Me, Me}}$ and $\text{H}_2\text{L}^{\text{Me, } t\text{-Bu}}$, respectively, were used as the capping ligands. Interestingly, for an acetonitrile solution of compound 7, the mass spectral data in the positive-ion mode display the presence of both $\mu\text{-OH}$ (m/z 835.62) and $\mu\text{-OMe}$ (m/z 849.63) binuclear Mn^{III} species, with the former being a product of hydrolysis in solution ([Figure S2](#)). For compound 8, however, the OMe-bridged form in an acetonitrile solution exists exclusively as a hydroxido-bridged product, $[(\text{L}^{\text{Me, } t\text{-Bu}}\text{Mn}^{\text{III}})_2(\mu\text{-OH})]\text{BPh}_4$, as revealed from its ESI-MS (positive) data involving a molecular-ion peak at m/z 1003.24 ($[\text{M}^+]$; [Figure S3](#)). In the case of ligand $\text{H}_2\text{L}^{\text{t-Bu, t-Bu}}$, the product obtained is a powdery solid that also conforms as a μ -hydroxido compound, as revealed by ESI-MS ([Figure S4](#)). Isolation of the solid product remained elusive with the remaining ligands. Nevertheless, their solutions in methanol all correspond to μ -hydroxido products, as observed for compound 8 ([Figure S3](#)).

In the second step, the OMe-bridged (7 and 8) or hydroxido-bridged (with ligand $\text{H}_2\text{L}^{\text{t-Bu, t-Bu}}$) precursor compounds were allowed to react at room temperature in methanol under constant stirring with 2 mol equiv of H_2DBC .³⁵ For the OMe-bridged precursors, the addition of Et_3N (1 equiv) is essential at this stage for completion of this reaction. The presence of aerial O_2 is also mandatory in this step. We believe this extra amount of base is used up to hydrolyze the $[(\text{L}^{\text{R}_1, \text{R}_2}\text{Mn}^{\text{III}})_2(\mu\text{-OMe})]^+$ species to the corresponding hydroxido species $[(\text{L}^{\text{R}_1, \text{R}_2}\text{Mn}^{\text{III}})_2(\mu\text{-OH})]^+$, which is the active intermediate in this case. With the remaining ligands, the precursor μ -hydroxido compounds generated in situ in

methanol were allowed to react with H₂DBC exactly under similar conditions, as mentioned above except that the addition of base was not required at all in the latter cases. The products, including their yields obtained in all cases, were grossly the same when the reactions were carried out in a single step, as mentioned in the [Experimental Section](#).

It may be mentioned here that the isolation of complexes 1–6 is only possible when methanol is used as a solvent, as reported in their synthesis protocol. The compounds are stable at room temperature and have reasonably good solubility in dichloromethane.

The IR spectra of the complexes show all of the characteristic bands of the coordinated ligands. In [Figure S5](#) are shown the IR spectra of the two representative compounds 1 and 3 in the 1750–1100 cm⁻¹ region. Two strong and sharp bands appearing at 1606 and 1473 cm⁻¹ in the spectrum of compound 3 correspond to $\nu(\text{C}=\text{O})$ and $\nu(\text{O}-\text{CH}_3)$ stretching modes, respectively, due to the incorporation of a carbonyl group and a methoxy group in the BMOD⁻ ring of the oxidized dioxolene moiety. The spectra of 1 and 2 include strong bands at 1480 and 1490 cm⁻¹, respectively, which can be assigned to a C–O stretching vibration of the attached semiquinonato ligand.³⁶

Description of the Crystal Structures. Attempts have been made to determine the crystal and molecular structures of the precursor methoxy-bridged compounds 7 and 8. A perspective view of the molecular structure of 7 is displayed in [Figure 1](#). Unfortunately, because of poor crystal quality, the data collected with several alternative crystals of compound 8 are found to be not enough to generate a molecular structure of publishable quality. However, an ORTEP view of a poorly refined structure is displayed in [Figure S6](#) for the purpose of its authentication. Complex 7 crystallizes in triclinic space group *P* $\bar{1}$ with two molecular mass units accommodated per unit cell ([Table S1](#)) and relevant metrical parameters, as summarized in [Table S2](#). The asymmetric unit consists of one [(L^{Me,Me}Mn^{III})₂(μ -OMe)]⁺ complex cation and one tetraphenylborate anion. The Mn^{III} centers in this cation are surrounded by N₂O₄ donor sets, providing distorted octahedral geometry for the metal centers. These include N₂O₂ coordination sites, all coming from the capping ligand [L^{Me,Me}]²⁻, together with a pair of O donor atoms coming from a bridging phenolate and a bridging methoxy anion, respectively. The basal plane around Mn1 is made up of N1, O1, O3, and O4 donor atoms (N3, O2, O3, and O5 for Mn2), and the apical sites are occupied by N2 and O2 atoms (N4 and O1 for Mn2). The two Mn centers are connected by a bridging methoxy (O3) and two bridging phenoxo (O1 and O2). O atoms The Mn1...Mn2 separation is 2.9393(12) Å. The methoxy O3 atom is almost equidistant [1.951(3) and 1.958(3) Å] from the individual Mn centers, which are high-spin d⁴ species showing Jahn–Teller axial elongations along the N2–Mn1–O2 and N4–Mn2–O1 axes, as revealed from the metrical data summarized in [Table S2](#).

The molecular structures and atom-labeling schemes for the semiquinonato complexes 1 and 2 are shown in [Figures 2](#) and [S7](#), respectively. Their metrical data provide confirmatory evidence in support of the semiquinonato status of the dioxolene moieties in these compounds. Identical atom-labeling schemes have been adopted for both structures for an easy comparison of their relevant metrical parameters ([Table 1](#)). The crystal structure of complex 1, which crystallizes in monoclinic space group *P*2₁ (*P* $\bar{1}$ for 2) with two molecular mass units accommodated per unit cell, is described here as a

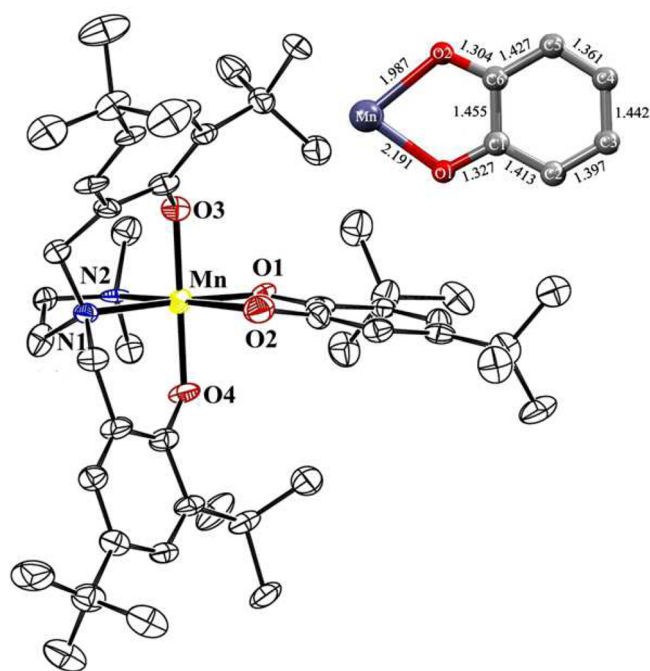


Figure 2. Molecular structure and atom-labeling scheme for complex 1 with thermal ellipsoids drawn at the 30% probability level. Inset: Observed bond lengths in the coordinated dioxolene moiety in 1.

Table 1. Selected Bond Distances (Å) and Angles (deg) for 1 and 2

	1	2
	Bond Lengths (Å)	
Mn–O1	1.986(5)	2.042(2)
Mn–O2	2.191(7)	2.108(2)
Mn–O3	1.882(5)	1.893(2)
Mn–O4	1.914(5)	1.869(2)
Mn–N1	2.086(6)	2.112(2)
Mn–N2	2.335(7)	2.304(3)
C1–O1	1.304(11)	1.304(4)
C6–O2	1.326(10)	1.271(3)
C1–C2	1.428(11)	1.404(4)
C2–C3	1.361(13)	1.362(5)
C3–C4	1.441(12)	1.414(5)
C4–C5	1.397(11)	1.364(4)
C5–C6	1.413(13)	1.437(4)
C6–C1	1.455(13)	1.447(4)
	Bond Angles (deg)	
O3–Mn1–O4	178.1(3)	173.55(9)
O2–Mn1–N2	167.5(2)	177.46(9)
O1–Mn1–N1	171.3(3)	173.93(9)

representative example for these two compounds. The asymmetric unit consists of a neutral mononuclear entity [Mn(L^{*t*-Bu,*t*-Bu})(DBSQ)]¹⁹ and two methanol molecules as solvents of crystallization. The Mn^{III} center in this complex has a distorted octahedral geometry. The basal positions are taken up by O3, N1, and O4 donor atoms, all coming from the N₂O₂ ligand, together with the O1 atom from the dioxolene moiety, while the apical positions are taken up by the donor atom O2, the remaining O donor atom from the dioxolene and N2 from the tetradentate ligand. The trans angles N2–Mn–O2 167.5(2)° [177.46(9)° for 2], N1–Mn–O1 171.3(3)° [173.93(9)°], and O3–Mn–O4 178.1(3)° [173.55(9)°] are

Table 2. Selected Bond Distances (Å) and Angles (deg) for 3–6

	3	4	5	6
	Bond Lengths (Å)			
Mn–O1	1.964(3)	1.9531(18)	1.941(5)	1.921(4)
Mn–O2	2.254(3)	2.2102(19)	2.211(5)	2.223(4)
Mn–O3	1.875(2)	1.8977(19)	1.905(4)	1.882(4)
Mn–O4	1.861(2)	1.8671(19)	1.888(4)	1.863(4)
Mn–N1	2.109(3)	2.113(2)	2.098(5)	2.091(5)
Mn–N2	2.310(3)	2.308(2)	2.309(6)	2.291(5)
C1–O1	1.315(4)	1.331(3)	1.315(8)	1.323(6)
C6–O2	1.226(4)	1.244(3)	1.239(8)	1.242(7)
C1–C2	1.339(5)	1.350(4)	1.352(10)	1.317(8)
C2–C3	1.485(6)	1.494(4)	1.476(12)	1.482(9)
C3–C4	1.517(5)	1.497(4)	1.486(13)	1.465(10)
C4–C5	1.315(5)	1.337(4)	1.359(11)	1.346(9)
C5–C6	1.473(5)	1.474(4)	1.500(10)	1.476(8)
C6–C1	1.496(5)	1.476(4)	1.432(10)	1.475(8)
	Bond Angles (deg)			
O3–Mn1–O4	176.94(12)	175.53(8)	174.7(2)	174.06(11)
O2–Mn1–N2	175.16(11)	174.93(8)	167.74(19)	177.11(9)
O1–Mn1–N1	174.44(11)	176.56(9)	171.1(2)	174.03(10)
O5–C3–C2	111.0(4)	110.5(3)	111.7(8)	111.2(3)
O5–C3–C4	108.8(4)	107.9(2)	107.4(8)	108.8(3)
O5–C3–C29	105.4(4)	104.5(2)	100.0(6)	103.8(3)
C2–C3–C29	110.8(4)	110.9(3)	113.6(9)	110.0(3)
C4–C3–C29	110.4(4)	110.3(3)	110.6(8)	109.9(4)
C2–C3–C4	110.4(4)	112.4(3)	112.7(7)	112.8(3)
C1–C2–C3	125.4(4)	123.4(3)	124.6(8)	123.5(4)
C1–C6–C5	119.4(4)	120.5(2)	120.2(6)	120.6(3)
C2–C1–C6	119.0(4)	119.4(3)	119.2(6)	119.6(3)
C4–C5–C6	117.1(4)	116.7(3)	118.7(7)	115.7(3)
C5–C4–C3	128.2(4)	126.8(3)	124.3(8)	127.2(3)

close to linearity, as expected for an octahedral geometry. The average Mn–O and Mn–N distances in the basal plane are well within the expected range.³⁷ The apical Mn–O2 2.191(7) Å [2.108(2) Å] and Mn–N2 2.335(7) Å [2.304(3) Å] distances, on the other hand, are significantly elongated because of high-spin Mn^{III} being a Jahn–Teller ion.³⁷

For a coordinated dioxolene moiety, the average C–O distance often provides decisive clues as to the oxidation state of this noninnocent ligand. The observed C–O distances are usually short (ca. 1.28 Å)^{38,39} when the ligand is in the quinone or semiquinone state compared to a fully reduced catecholate ligand (ca. 1.34 Å).⁴⁰ The average C–O distance observed here is 1.315 Å (1.287 Å). Considering that the crystal structure of **1** has been determined at 150 K⁴¹ and that of **2** at a much higher temperature of 293 K, the C–O distance in **1** is somewhat in the upper range (due to charge transfer from a near phenolate as discussed in the mechanistic part; see later). Apart from this, the observation of a two short–four long intraring C–C bond pattern (quinoid distortion) provides confirmatory evidence (inset, Figure 2) in support of the semiquinone status for the dioxolene moiety^{39a} in compounds **1** and **2**.

Compounds **3–6** have a different set of structures, as established from their X-ray crystallographic analysis. These are all isostructural molecules. While **3** crystallizes in the triclinic space group $P\bar{1}$ with two molecular mass units accommodated per cell, compounds **4–6**, on the other hand, have the monoclinic space group $P2_1/c$ in all cases with four molecular mass units in their respective unit cell. Their relevant metrical parameters are summarized in Table 2. Identical atom-labeling

schemes have also been adopted here for all of these structures in order to have a straightforward comparison of their relevant metrical data. Again, for the sake of brevity, a generic description of these structures will be provided considering compound **3** as a representative example. A perspective view of the molecular structure of **3** is depicted in Figure 3, and those

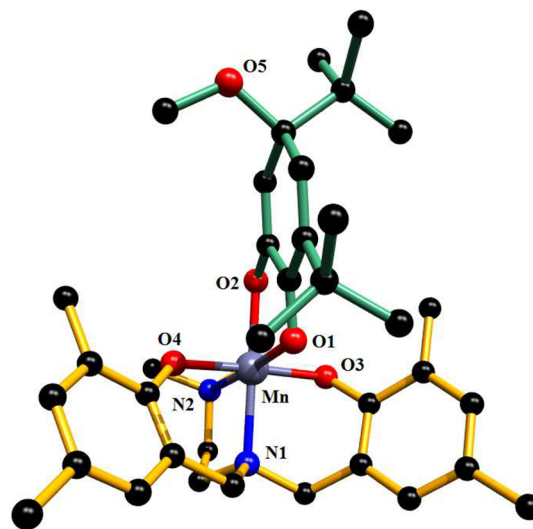


Figure 3. Partially labeled POV-Ray (in ball-and-stick form) diagram showing the atom-labeling scheme in complex **3**. H atoms have been omitted for clarity.

of 4–6 are shown in Figures S8–S10, respectively. The Mn center is also six-coordinated here using a doubly deprotonated facially coordinating N_2O_2 ligand, providing N1, N2, O3, and O4 donor atoms and a mononegative dioxolene derivative (BMOD^-)¹⁹ with O1 and O2 donors to complete the octahedral geometry. The Mn–O [1.861(2)–1.964(3) Å] and Mn–N [2.091(5)–2.113(2) Å] distances in the basal plane in these compounds are all in the expected range.³⁷ The dioxolene O2 atom occupies the Jahn–Teller axis, together with the imino N2 atom of the tetradentate ligand, to form a trans O2–Mn–N2 angle of 175.16(11)°. The elongation along this axis is clearly reflected in the bond lengths Mn–O2 [2.254(3)–2.210(2) Å] and Mn–N2 [2.310(3)–2.291(5) Å], compared to the relevant bond distances in the equatorial plane (Table 2).

Perhaps the most striking feature observed in the structures of compounds 3–6 is the unprecedented type of dioxolene moiety observed in these molecules. As displayed in Figure 4,

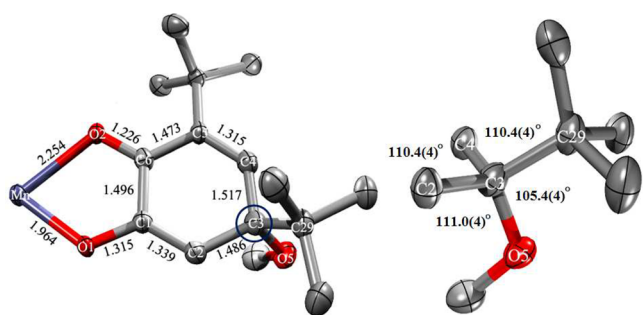


Figure 4. Bond lengths in the dearomatized dioxolene ring and bond angles at the sp^3 -hybridized C3 center in complex 3.

the intraring C–C distances and angles in the dioxolene ring changed drastically in these molecules during the course of their aerobic oxidation, followed by methanolysis. The C2–C3 1.485(6) Å, C3–C4 1.517(5) Å, C5–C6 1.473(5) Å, and C6–C1 1.496(5) Å bond lengths in 3 are almost of single-bond character, while those between C1–C2 1.339(5) Å and C4–C5 1.315(5) Å are close to double-bond character. Also, the C6–O2 distance 1.226(4) Å is more like a double bond, providing a planar quinoid structure that includes half of this ring (plane *a* in Figure 5) involving the C2, C1, C6, C5, and C4 atoms. The remaining half containing C2, C3, and C4 centers lie in a different plane (plane *b* in Figure 5), and together they provide a “half-chair”-like conformation for this ring, with planes *a* and *b* making a dihedral angle of 5.61°. The observed nonplanarity

breaks the aromaticity of this transformed dioxolene ring, which now includes a C3 center that makes the angles C2–C3–C4 110.4(4)°, C2–C3–O5 111.0(4)°, and C4–C3–C29 110.4(4)°, all deviating substantially from 120°, the expected angle at a C sp^2 center (Figure 4). The remaining angle at C3, O5–C3–C29, is 105.4(4)°, which is also close to an ideal tetrahedral bond angle of 109.5°. The data thus provide a clear indication that the hybridization status of the C3 atom in the ring has been changed to sp^3 from its initial sp^2 state in complexes 3–6 during the course of this oxidation, followed by a methanolysis reaction (see later).

Magnetic Susceptibility Data. The magnetic moment data obtained at room temperature for complexes 1–6 are put together in the Experimental Section. The semiquinonato compounds 1 and 2 display subnormal magnetic moments of 3.94 and 3.89 μ_{B} (per Mn), respectively, at 298 K. The observed decrease in the effective magnetic moments for these manganese(III) complexes below their $S = 2$ spin-only value of 4.86 μ_{B} is attributable to the strong antiferromagnetic interactions of the single unpaired electron of the coordinated semiquinone (DBSQ) moiety with the four manganese(III) unpaired electrons, producing an $S = 3/2$ ground state with an expected spin-only moment of 3.92 μ_{B} .⁴² Susceptibility data for the remaining compounds [$\text{Mn}^{\text{III}}(\text{L}^{\text{R}_1, \text{R}_2})(\text{BMOD})$] (3–6) containing a quinone derivative BMOD^- as the coligand, vary in the range 4.54–4.88 μ_{B} . The results are well in conformity with molecules behaving as a simple paramagnet with an $S = 2$ ground state.

Electronic Spectra. The electronic spectra of complexes 1–6 have closely similar features (Figure 6), each displaying a number of moderate-to-high-intensity bands in a dichloromethane solution, as summarized in Table 3. Spectra with similar features involving multiple charge-transfer bands are not uncommon for metal semiquinonato compounds.³⁶ Complexes 1 and 2 show a band of moderate intensity with $\epsilon = 1350 \text{ L mol}^{-1} \text{ cm}^{-1}$ (1550 $\text{L mol}^{-1} \text{ cm}^{-1}$ for 2) in the visible region at 700 nm (724 nm) with a vibronic progression that is diagnostic of a coordinated semiquinone ligand in these molecules.⁴³ The remaining strong band in the visible region at 488 nm (495 nm) with $\epsilon = 4200 \text{ L mol}^{-1} \text{ cm}^{-1}$ (4000 $\text{L mol}^{-1} \text{ cm}^{-1}$) possibly arises from the $\text{PhO}^- \rightarrow \text{Mn}^{\text{III}}$ ligand-to-metal charge-transfer transition arising from a $p\pi$ orbital on the phenolate O atom to the half-filled Mn^{III} $d\pi^*$ orbitals.⁴⁴ This band in complexes 3–6 is slightly red-shifted and appears in the form of a shoulder. All other bands appearing in the UV region in these complexes are due to ligand internal transitions.

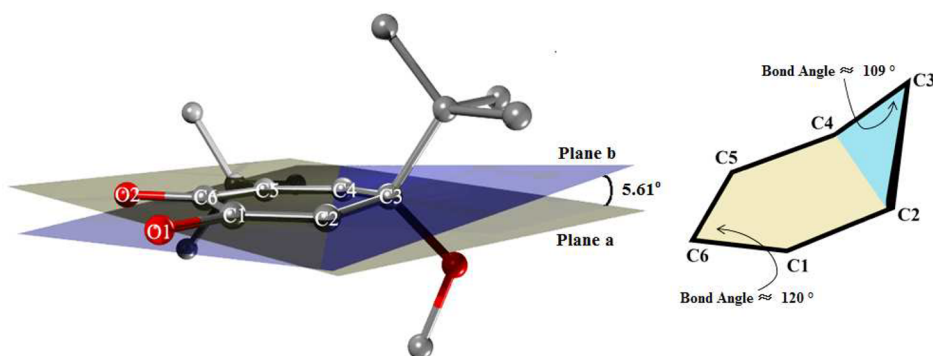


Figure 5. Dihedral angle between planes *a* and *b* in complex 3 and the half-chair conformation of the transformed dioxolene ring.

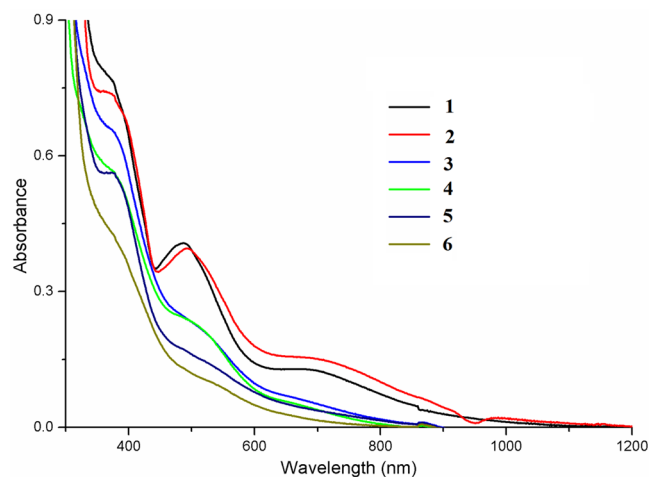


Figure 6. UV-vis spectra of the manganese(III) complexes (1–6) in a dichloromethane solution (concn $\sim 10^{-4}$ M).

Table 3. Electronic Spectra of Complexes 1–6

compound	λ , nm (ϵ , L mol ⁻¹ cm ⁻¹)
[Mn(L ^{t-Bu,t-Bu})(DBSQ)]·2CH ₃ OH (1)	292 (20000), 370 (7900), 488 (4200), 700 (1350)
[Mn(L ^{t-Bu,OMe})(DBSQ)]·CH ₃ OH (2)	303 (24200), 377 (7400), 495 (4000), 724 (1550)
[Mn(L ^{Me,Me})(BMOD)]·2CH ₃ OH (3)	281 (18500), 373 (6650), 505 (2900), 661 (660)
[Mn(L ^{Me,t-Bu})(BMOD)]·CH ₃ OH (4)	277 (17400), 374 (5700), 509 (2300), 660 (550)
[Mn(L ^{t-Bu,Me})(BMOD)] (5)	289 (14900), 375 (5650), 511 (1550)
[Mn(L ^{Cl,Cl})(BMOD)]·H ₂ O (6)	287 (13000), 376 (4150), 523 (1100)

Electrochemical Properties. Because the substituent combinations R₁ and R₂ in the capping ligand H₂L^{R₁,R₂} play the domineering role in deciding the course of these redox reactions, we thought it would be prudent to study the electrochemical behaviors of complexes 1–6, just to explore how these substituents in the capping ligand influence their overall redox performances. Cyclic voltammograms of the complexes as well as their free associated capping ligands have been recorded at a glassy carbon working electrode under an atmosphere of purified dinitrogen in a DCE solution (0.1 M TBAP) at 25 °C in the potential range of –1.0 to +1.8 V versus Ag/AgCl reference electrode. The voltammetric features of the free ligands H₂L^{t-Bu,t-Bu} and H₂L^{t-Bu,OMe} are quite similar, with both undergoing a single oxidation process in the anodic potential range and with the degree of reversibility being compromised upon going from H₂L^{t-Bu,OMe} to H₂L^{t-Bu,t-Bu}. We believe that the quasi-reversible voltammogram observed at $E_{1/2} = +0.72$ V ($\Delta E = 143$ mV) with the ligand H₂L^{t-Bu,t-Bu} [Figure 7 (inset)] is due to phenolate \rightarrow phenoxyl oxidation. The corresponding oxidation for H₂L^{t-Bu,OMe} is grossly reversible, appearing at a less positive potential of 0.45 V ($\Delta E = 80.2$ mV). The ease of oxidation in the latter case is due to the strong electron-donating influence of the OMe group in the para position of the phenolate ring in the ligand. These two ligands are known for their ability to form the semiquinonato complexes 1 and 2. The cyclic voltammogram of complex 1 in the anodic potential range is displayed in Figure 7, which involves two electrochemical processes (processes I and II). Similar features are also observed with compound 2. Process I is a quasi-reversible oxidation appearing at $E_{1/2} = 0.53$ V ($\Delta E_p =$

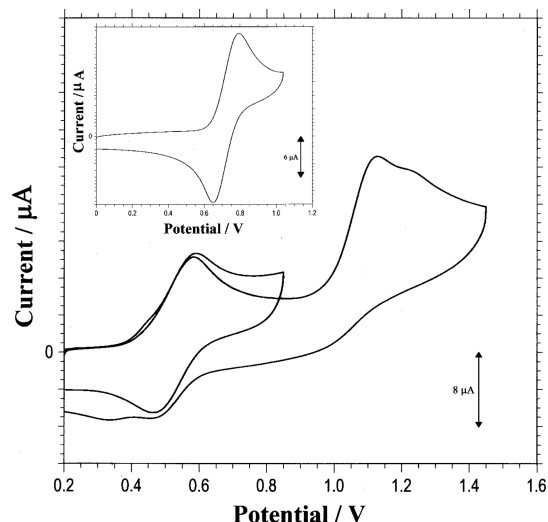


Figure 7. Cyclic voltammogram of compound 1 in DCE (0.1 M TBAP) at a scan rate of 100 mV s⁻¹ using a glassy carbon working electrode (potentials vs Ag/AgCl). Inset: Cyclic voltammogram of the corresponding free ligand H₂L^{t-Bu,t-Bu} in DCE.

126 mV) [0.44 V (184 mV) for 2], followed by an irreversible oxidation (process II) at $E_{pa} = 1.12$ V (0.75 V). The data, as expected, clearly indicate that the oxidation processes are much easier with compound 2 than with compound 1. Taking a cue from the electrochemical data of the free ligands, one can conclude that process I in this case is most likely to originate from a ligand-based oxidation involving one of the phenolate moieties of the capping ligand [L^{t-Bu,t-Bu}]²⁻ (or [L^{t-Bu,OMe}]²⁻). The absence of the cathodic response in process II confirms the onset of a decomposition process after the initial oxidation. In the cathodic region, the cyclic voltammograms of 1 and 2 involve a couple of irreversible reductions. In order to avoid speculation, we have decided not to make any further comments about these electrochemical processes.

The electrochemical behaviors of complexes 3–6 are grossly similar but differ widely from those of complexes 1 and 2. In fact, the cyclic voltammograms of the free capping ligands associated with these compounds show a lone irreversible oxidation, with E_{pa} lying in the range between 0.7 and 0.8 V. The voltammogram of a representative ligand H₂L^{Me,t-Bu} is shown in the inset of Figure S11. The results suggest the instability of the oxidized phenoxyl moiety of these ligands in the voltammetric time scale and fail to reappear during the reverse cathodic scan. The cyclic voltammogram of the corresponding dioxolene compound 4 is also shown in Figure S11 as a representative of the BMOD-type compounds. It constitutes three irreversible oxidations in the observed potential range. To avoid any speculative remarks, we have decided to make no further comment about the origin of these oxidation processes.

The results of the electrochemical study thus indicate that the stability of the phenoxyl moiety of the oxidized capping ligand in 1–6 is probably the key in deciding the course of either of the two oxidation reactions. The ligands H₂L^{t-Bu,t-Bu} and H₂L^{t-Bu,OMe}, which can generate stable phenoxyl radicals at least in the voltammetric time scale, are capable of producing the semiquinonato compounds 1 and 2. The rest of the ligands, on the other hand, are incapable of generating the stable phenoxyl radicals and guide the reaction to proceed to the

generation of compounds 3–6, with BMOD as the oxidized dioxolene moiety.

Ligand-Induced Tuning of the Oxidase Activity: Two-Electron versus Four-Electron Reduction of Molecular Oxygen. We are now quite certain that a binuclear μ -hydroxidomanganese(III) cationic complex, $[(L^{R_1,R_2}Mn^{III})_2(\mu-OH)]^+$, is initially formed as an intermediate when the ligand $H_2L^{R_1,R_2}$, together with H_2DBC , is allowed to react with $Mn(ClO_4)_2 \cdot 6H_2O$ in methanol in the mandatory presence of a base and molecular oxygen. This intermediate (its μ -OMe derivative is isolable as a crystalline solid with the ligands $H_2L^{Me,Me}$ and $H_2L^{Me,t-Bu}$ using tetraphenylborate as the counteranion) then participates in the oxidation of H_2DBC in the presence of molecular oxygen as an electron acceptor and is reduced by two or four electrons (eqs 1 and 2) depending on the substituent combination (R_1 and R_2) present in the attached capping ligand $[L^{R_1,R_2}]^{2-}$. Thus, with the t -Bu, t -Bu and t -Bu, OCH_3 combinations, the incoming DBC^{2-} ligand is oxidized up to the semiquinone $DBSQ^-$ stage to generate compounds 1 and 2, respectively, and in the process, molecular oxygen is reduced to H_2O_2 (eq 1). The generation of H_2O_2 during this oxidation was monitored spectrophotometrically following a reported iodometric detection procedure,^{23,24} as outlined in the Experimental Section. This involves the development of a characteristic UV band due to the $\pi_g \rightarrow \sigma_u^*$ transition⁴⁵ for I_3^- ($\lambda_{max} = 353$ nm; $\epsilon = 26\,000$ L mol⁻¹ cm⁻¹) when the generated H_2O_2 is allowed to react with I^- at pH = 2.0. Figure 8 depicts the time-interval spectra for the

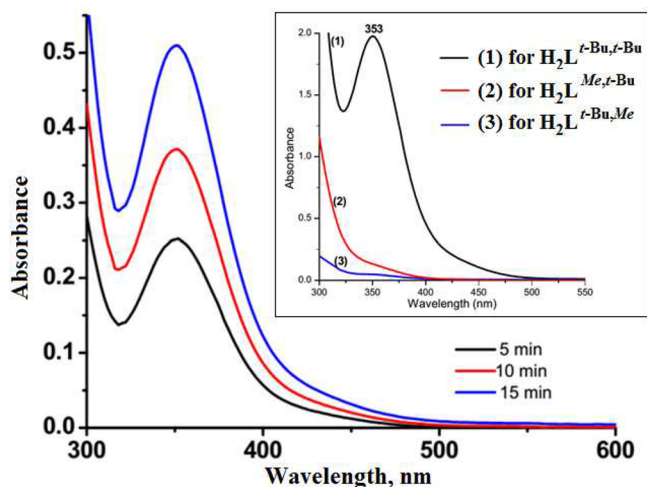
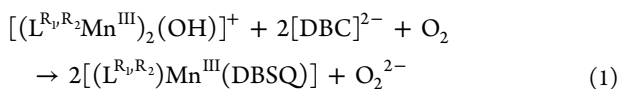


Figure 8. Time-interval spectra that show the indirect monitoring (iodometric assay; details are in the text) of the gradual accumulation of H_2O_2 in solution during the synthesis of complex 1. Inset: Complete absence of H_2O_2 generation in solution when the capping ligand is changed from $H_2L^{t-Bu,t-Bu}$ to $H_2L^{Me,t-Bu}$ or $H_2L^{t-Bu,Me}$.

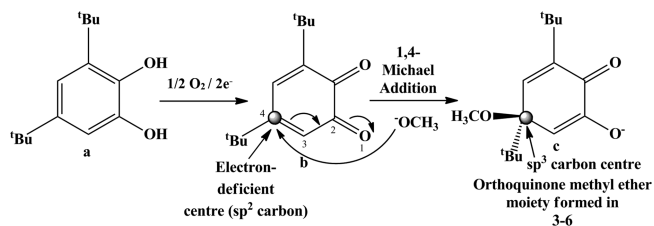
gradually generated I_3^- in solution over a period of ca. 15 min. The data provide an indirect estimation of H_2O_2 accumulated during the synthesis of compound 1 following eq 1.



Interestingly, with the rest of these ligands under similar experimental conditions, we failed to detect any H_2O_2 in the reaction mixtures, as shown in Figure 8 (inset) for compounds 4 and 5. We believe molecular oxygen in the latter instant is

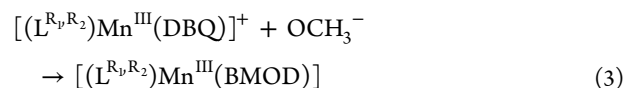
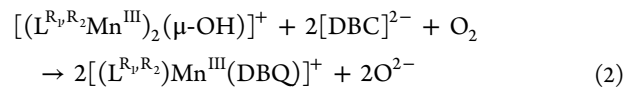
acting as a four-electron oxidant that oxidizes the incoming dioxolene moiety up to the quinone (DBQ)¹⁹ stage and itself is reduced to water, as shown by eq 2. The coordinated o -quinone in these compounds appears to be highly reactive^{46a} and initiates a domino reaction that involves an intermolecular Michael-type 1,4-addition⁴⁶ with a methoxy group as a nucleophile from the solvent methanol (eq 3), as outlined in Scheme 2. The products obtained (3–6) are very interesting

Scheme 2. Domino Reaction Involving a Michael-Type 1,4-Addition of the CH_3O^- Group to the Orthoquinone Moiety Generated during the Four-Electron Reduction of O_2 by the Catecholato Ligand That Led to the Formation of Compounds 3–6^a



^aParticipation of the Mn^{III} ion in the reaction is not shown.

molecules, containing an unusual type of nonplanar oxidized dioxolene moiety that forms part of the methyl ether derivative $BMOD^-$.



In order to have further verification of our conjecture that the formation of a quinoid-type molecule $[L^{R_1,R_2}Mn^{III}(DBQ)]^+$ is the initial step of the domino reaction that leads to the final products $[L^{R_1,R_2}Mn^{III}(BMOD)]$ (3–6), we attempted the syntheses of 3–6, following an alternative route (method B in the Experimental Section) in which H_2DBC was replaced by DBQ^{19} as the precursor dioxolene moiety. The successful isolation of 3–6 in moderate-to-high yields from a methanol solution confirms the involvement of the quinoid compound $[L^{R_1,R_2}Mn^{III}(DBQ)]^+$ as the precursor to the final products 3–6.

We believe this two- versus four-electron reduction of O_2 by the μ -hydroxido intermediates $[(L^{R_1,R_2}Mn^{III})_2(\mu-OH)]^+$ (Scheme 1) is fine-tuned by the secondary coordination sphere around the Mn^{III} centers, which differ among themselves by the substituent combinations (R_1 and R_2) in the phenolate arms of the capping ligands. It is well-known that both 2,4-di-*tert*-butylphenol and 2-*tert*-butyl-4-methoxyphenol can efficiently stabilize the phenoxyl radical because of their ability to accept the spin density from the associated ring.⁴⁷ The presence of these phenolate moieties in the attached $[L^{R_1,R_2}]^{2-}$ ligands in 1 and 2 stabilizes the dioxolene moiety in the semiquinone form (DBSQ) during their oxidation because of an extended charge delocalization between the phenolate and semiquinone moieties via participation of the appropriate metal orbital(s). An equilibrium between the semiquinone/phenolate (form A) and catecholate/phenoxyl (form B) tautomeric forms (Figure 9) provides extra stability to the semiquinoid structures in 1 and 2 and thus restricts the oxidase activity up to the two-

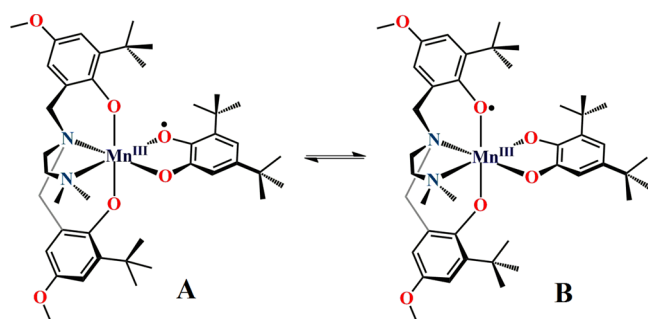


Figure 9. Equilibrium between the tautomeric forms involving the semiquinone/phenolate (form A) and catechol/phenoxyl (form B) combinations.

electron stage. A careful look at the crystal structure of the phenolate moiety (Table S3) in compound **1** (Figure 10)

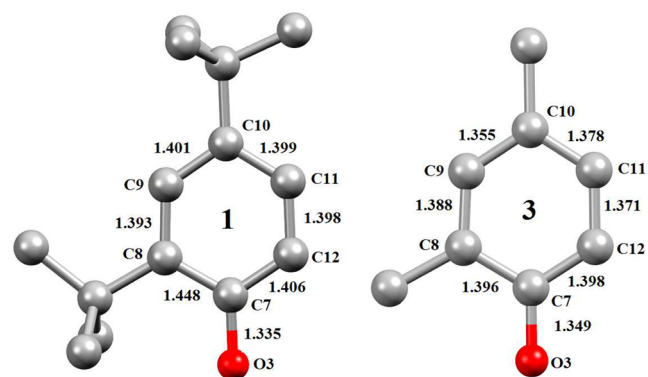


Figure 10. Comparison between the relevant bond distances of the phenolate moieties in complexes **1** and **3**. Enlargement of the C7–C8 bond in complex **1** provides an indication of the partial phenoxyl character of the concerned phenol ring.

determined at lower temperature (150 K)⁴¹ indicates an enlarged C8–C7 bond of 1.448 Å compared to the

corresponding bond distance (1.396 Å) in **3**, providing a clear indication that the phenolate ring in **1** is displaying a partial quinoid distortion characteristic of a phenoxyl moiety.⁴⁸ The shift of the odd phenolate electron to the semiquinone ring is also reflected in elongation of the average C–O distance (1.315 Å; Table 1) in the dioxolene moiety of compound **1**. Thus, the overall structure of **1** at lower temperature (150 K) is a combination of both forms A and B, with form B being the major contributor. Also, the appearance of a distinct signal at 1631 cm⁻¹ in the IR spectrum of compound **1** (Figure S5) due to the $\nu(\text{C}=\text{C})$ stretching pattern provides an indication of the presence of a phenoxyl moiety in this compound.⁴⁹ Thus, of the two tautomeric forms, the structure B probably contributes more to the overall structures of compounds **1** and **2**. For the remaining compounds, O₂ reduction is not arrested in the two-electron stage because of the poor stability of the intermediate semiquinonato compound. That probably explains why only a few semiquinonato compounds of manganese(III) have been reported thus far in the literature.^{43a,50} Dioxolene oxidation during the formation of compounds **3**–**6** proceeds further up to the quinonato stage with concomitant four-electron reduction of O₂.

Krebs et al.^{18c} recently reported a series of mononuclear manganese(III) complexes using tetradentate tripodal ligands with N₄ and N₃O donor combinations with closely related structures. Some of these compounds satisfactorily model the structure of a manganese-substituted form of an intradiol-cleaving iron catechol dioxygenase. These complexes also exhibit high catalytic activity for the oxidation of 3,5-di-*tert*-butylcatechol to 3,5-di-*tert*-butylquinone, mimicking the role of catechol oxidase model compounds showing saturation kinetics at high substrate concentrations. Interestingly, the oxidized dioxolene moiety did not bind the Mn^{III} center in those compounds, as observed with compounds **1**–**6**.

DFT Calculations. Theoretical IR spectra for representative types of these reported complexes have been constructed on the basis of DFT calculations (Figure S12). Relevant vibrational bands of these spectra have been used subsequently for

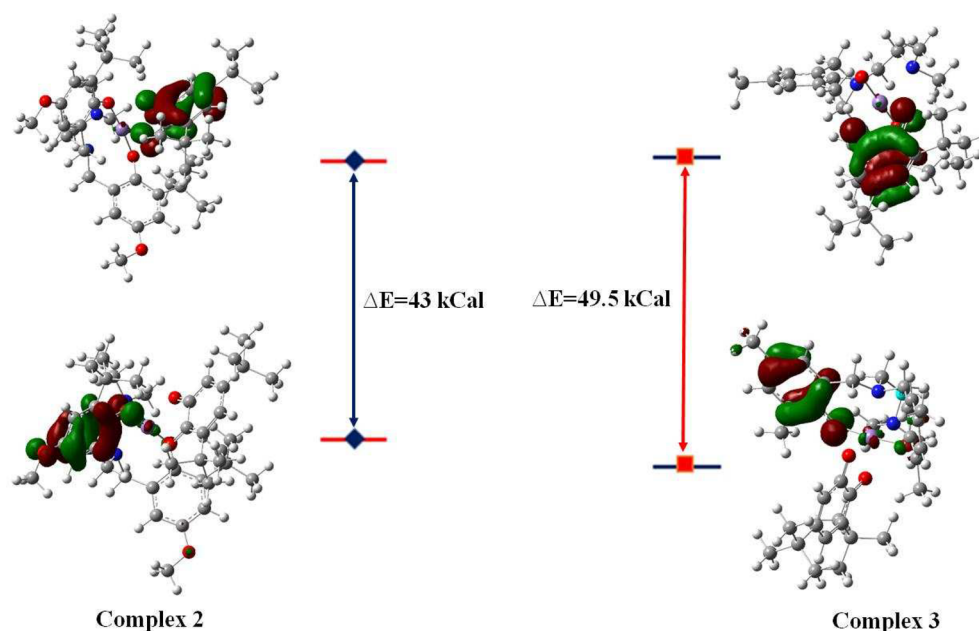


Figure 11. Energy gaps between the phenolate-based HOMO and semiquinone-based LUMO in complexes **2** and **3**.

correlation with the corresponding experimental spectra. For example, the C–O stretching vibration of the semiquinonato moiety in compound **1** appears at 1497 cm⁻¹ in its theoretical spectrum (video S1). Unfortunately, in the experimental spectrum, this region is quite congested because of the appearance of three strong bands, including the one at 1480 cm⁻¹, which shows a fair degree of concordance with the theoretical C–O vibration. The DFT-optimized complex [Mn^{III}(L^{Me,Me})(DBQ)] interestingly exhibits an IR band at 1606 cm⁻¹ due to the C=O stretching vibration of the associated quinone moiety (video S2), which is in complete agreement with the experimental C=O vibration of the [Mn^{III}(L^{Me,Me})(BMOD)] complex (**3**).

We also performed DFT calculations on complex **2** and the optimized semiquinone structure of compound [Mn^{III}(L^{Me,Me})-(DBSQ)], only to see that the semiquinone ring in complex **2** is richer in electron density likely because of the shift of the electron density from the associated phenolate ring. Accordingly, the spin density on the phenolate ring is more for **2**, suggesting greater phenoxyl character in **2** relative to **3** (Figure 11). Further, it is found that the energy separation between the phenolate-based highest occupied molecular orbital (HOMO) and the semiquinone-based lowest unoccupied molecular orbital (LUMO) is ~6.5 kcal lower for **2** relative to **3**. Thus, the higher stability of compound **2** in its semiquinone form is likely due to the extended delocalization of the electron density over both phenolate and semiquinone rings. For complex **3**, however, the unstable semiquinonato intermediate undergoes further oxidation, followed by a Michael-type addition reaction to the final BMOD product.

CONCLUDING REMARKS

In summary, we have reported here the oxidase activity of binuclear μ -hydroxidodimanganese(III) cationic intermediates [(L^{R₁,R₂}Mn^{III})₂(μ -OH)]⁺, which, during their reaction with H₂DBC, exhibit either a two- or four-electron reduction of O₂. The course of these alternative reactions appears to be controlled by the secondary coordination sphere surrounding the Mn^{III} centers in the μ -hydroxido intermediates (Scheme 1). The presence of 2,4-di-*tert*-butylphenol and 2-*tert*-butyl-4-methoxyphenol moieties in the [H₂L^{R₁,R₂}] ligands in **1** and **2**, respectively, stabilizes the dioxolene moiety in the semiquinone form⁴⁷ during their oxidation because of an extended charge delocalization between the phenolate and semiquinone moieties (Figure 9). For the remaining compounds, O₂ reduction is not arrested in the two-electron stage because of the poor stability of the intermediate semiquinonato products. The oxidation of dioxolene proceeds further up to the quinonato stage with concomitant four-electron reduction of O₂. The reactive quinonato compounds then participate in a domino reaction with the solvent methanol to provide compounds **3**–**6** with an unusual dioxolene moiety (Scheme 2). The present work thus provides a unique example of the influence of the secondary coordination sphere in controlling the electron stoichiometry of the oxidase action.

ASSOCIATED CONTENT

Supporting Information

The Supporting Information is available free of charge on the ACS Publications website at DOI: 10.1021/acs.inorgchem.7b00147.

¹H NMR spectrum of the ligand H₂L^{f-Bu,OMe} (Figure S1), ESI-MS spectra in the positive-ion mode of compounds **7** and **8** (Figures S2 and S3) and of the intermediate [(L^{f-Bu,f-Bu}Mn^{III})₂(μ -OH)]⁺ (Figure S4), IR spectra of **1** and **3** (Figure S5), partially labeled perspective views of the crystal structures of complexes **2**, **4**–**6** and **8** (Figures S6–S10), cyclic voltammograms of compound **4** and the ligand H₂L^{Me,f-Bu} (Figure S11), theoretical FT-IR spectra of the DFT-optimized complexes **1** and [Mn^{III}(L^{Me,Me})-(DBQ)] (Figure S12), relevant crystallographic data (Table S1), metrical parameters for compound **7** (Table S2), selected bond distances of phenolate rings in **1**–**6** (Table S3), and details of the syntheses and characterization of the H₂L^{R₁,R₂} ligands (PDF)

Video presentation of the C–O stretchings of the DFT-optimized complex **1** (video S1) (AVI)

Video presentation of the C–O stretchings of the DFT-optimized complex [Mn^{III}(L^{Me,Me})(DBQ)] (video S2) (AVI)

Accession Codes

CCDC 1548156–1548162 contain the supplementary crystallographic data for this paper. These data can be obtained free of charge via www.ccdc.cam.ac.uk/data_request/cif, or by emailing data_request@ccdc.cam.ac.uk, or by contacting The Cambridge Crystallographic Data Centre, 12 Union Road, Cambridge CB2 1EZ, UK; fax: +44 1223 336033.

AUTHOR INFORMATION

Corresponding Author

*E-mail: icmc@iacs.res.in.

ORCID

Muktimoy Chaudhury: 0000-0002-6069-1072

Notes

The authors declare no competing financial interest.

ACKNOWLEDGMENTS

We thank Dr. Abhishek Dey for his help with DFT calculations. We also thank the reviewers for providing many constructive suggestions. This work was supported by the Council of Scientific and Industrial Research (CSIR), New Delhi, India. D.M. and M.C.M. also thank the CSIR for the award of research fellowships. Single-crystal X-ray diffraction data were recorded on an instrument supported by DST, New Delhi, India, as a National Facility at IACS under the IRHPA program.

REFERENCES

- (1) Simandi, L. Í. *Advances in Catalytic Activation of Dioxygen by Metal Complexes*; Catalysis by Metal Complexes 26; Kluwer Academic Publishers: Dordrecht, The Netherlands, 2002.
- (2) (a) Arakawa, H.; Aresta, M.; Armor, J. N.; Barteau, M. A.; Beckman, E. J.; Bell, A. T.; Bercaw, J. E.; Creutz, C.; Dinjus, E.; Dixon, D. A.; Domen, K.; DuBois, D. L.; Eckert, J.; Fujita, E.; Gibson, D. H.; Goddard, W. A.; Goodman, D. W.; Keller, J.; Kubas, G. J.; Kung, H. H.; Lyons, J. E.; Manzer, L. E.; Marks, T. J.; Morokuma, K.; Nicholas, K. M.; Periana, R.; Que, L., Jr.; Rostrup-Nielsen, J.; Sachtler, W. M. H.; Schmidt, L. D.; Sen, A.; Somorjai, G. A.; Stair, P. C.; Stults, B. R.; Tumas, W. Catalysis research of relevance to carbon management: progress, challenges, and opportunities. *Chem. Rev.* **2001**, *101*, 953–996. (b) Shilov, A. E.; Shul'pin, G. B. Activation of C–H bonds by metal complexes. *Chem. Rev.* **1997**, *97*, 2879–2932.
- (3) (a) Solomon, E. I.; Heppner, D. E.; Johnston, E. M.; Ginsbach, J. W.; Cirera, J.; Qayyum, M.; Kieber-Emmons, M. T.; Kjaergaard, C. H.; Hadt, R. G.; Tian, L. Copper active sites in biology. *Chem. Rev.* **2014**,

- 114, 3659–3853. (b) Kosman, D. J. Multicopper oxidases: a workshop on copper coordination chemistry, electron transfer, and metallophysiology. *J. Biol. Inorg. Chem.* **2010**, *15*, 15–28. (c) Battaini, G.; Granata, A.; Monzani, E.; Gullotti, M.; Casella, L. Biomimetic oxidations by dinuclear and trinuclear copper complexes. *Adv. Inorg. Chem.* **2006**, *58*, 185–233. (d) Rosenzweig, A. C. Bioinorganic chemistry: zeroing in on a new copper site. *Nat. Chem.* **2009**, *1*, 684–685.
- (4) (a) Ferguson-Miller, S.; Babcock, G. T. Heme/copper terminal oxidases. *Chem. Rev.* **1996**, *96*, 2889–2908. (b) Kaila, V. R. L.; Verkhovskiy, M. I.; Wikstrom, M. Proton-coupled electron transfer in cytochrome oxidase. *Chem. Rev.* **2010**, *110*, 7062–7081.
- (5) (a) Cracknell, J. A.; Vincent, K. A.; Armstrong, F. A. Enzymes as working or inspirational electrocatalysts for fuel cells and electrolysis. *Chem. Rev.* **2008**, *108*, 2439–2641. (b) Adler, S. B. Factors governing oxygen reduction in solid oxide fuel cell cathodes. *Chem. Rev.* **2004**, *104*, 4791–4844. (c) Markovic, N. M.; Schmidt, T. J.; Stamenkovic, V.; Ross, P. N. Oxygen reduction reaction on Pt and Pt bimetallic surfaces: a selective review. *Fuel Cells* **2001**, *1*, 105–116.
- (6) (a) Egami, H.; Oguma, T.; Katsuki, T. Oxidation catalysis of Nb (salan) complexes: asymmetric epoxidation of allylic alcohols using aqueous hydrogen peroxide as an oxidant. *J. Am. Chem. Soc.* **2010**, *132*, 5886–5895. (b) Hermans, I.; Spier, E. S.; Neuenschwander, U.; Turra, N.; Baiker, A. Selective oxidation catalysis: opportunities and challenges. *Top. Catal.* **2009**, *52*, 1162–1174.
- (7) (a) Fukuzumi, S.; Tahsini, L.; Lee, Y.-M.; Ohkubo, K.; Nam, W.; Karlin, K. D. Factors that control catalytic two-versus four-electron reduction of dioxygen by copper complexes. *J. Am. Chem. Soc.* **2012**, *134*, 7025–7035. (b) Kakuda, S.; Rolle, C. J.; Ohkubo, K.; Siegler, M. A.; Karlin, K. D.; Fukuzumi, S. Lewis acid-induced change from four- to two-electron reduction of dioxygen catalyzed by copper complexes using scandium triflate. *J. Am. Chem. Soc.* **2015**, *137*, 3330–3337. (c) Gennari, M.; Brazzolotto, D.; Pécaut, J.; Cherrier, M. V.; Pollock, C. J.; DeBeer, S.; Retegan, M.; Pantazis, D. A.; Neese, F.; Rouzières, M.; Clérac, R.; Duboc, C. Dioxygen activation and catalytic reduction to hydrogen peroxide by a thiolate-bridged dimanganese(II) complex with a pendant thiol. *J. Am. Chem. Soc.* **2015**, *137*, 8644–8653.
- (8) (a) *Biomimetic Oxidations Catalyzed by Transition Metal Complexes*; Meunier, B., Ed.; Imperial College Press: London, 2000. (b) *Oxygen Complexes and Oxygen Activation by Transition Metals*; Martell, A. E., Sawyer, D. T., Eds.; Plenum: New York, 1988.
- (9) (a) Costas, M.; Mehn, M. P.; Jensen, M. P.; Que, L., Jr. Dioxygen activation at mononuclear nonheme iron active sites: enzymes, models, and intermediates. *Chem. Rev.* **2004**, *104*, 939–986. (b) Puri, M.; Que, L., Jr. Toward the synthesis of more reactive S = 2 non-heme oxoiron (IV) complexes. *Acc. Chem. Res.* **2015**, *48*, 2443–2452. (c) Nam, W. High-valent iron (IV)-oxo complexes of heme and non-heme ligands in oxygenation reactions. *Acc. Chem. Res.* **2007**, *40*, 522–531.
- (10) (a) Hematian, S.; Garcia-Bosch, I.; Karlin, K. D. Synthetic heme/copper assemblies: toward an understanding of cytochrome c oxidase interactions with dioxygen and nitrogen oxides. *Acc. Chem. Res.* **2015**, *48*, 2462–2474. (b) Citek, C.; Herres-Pawlis, S.; Stack, T. D. P. Low temperature syntheses and reactivity of Cu₂O₂ active-site models. *Acc. Chem. Res.* **2015**, *48*, 2424–2433.
- (11) Sigel, A.; Sigel, H. *Manganese and its Role in Biological Processes. Metal Ions in Biological Systems*; Marcel Dekker: New York, 2000; Vol. 37.
- (12) (a) Hamberg, M.; Su, C.; Oliw, E. Manganese lipoyxygenase: discovery of a bis-allylic hydroperoxide as product and intermediate in a lipoyxygenase reaction. *J. Biol. Chem.* **1998**, *273*, 13080–13088. (b) Su, C.; Sahlin, M.; Oliw, E. H. Kinetics of manganese lipoyxygenase with a catalytic mononuclear redox center. *J. Biol. Chem.* **2000**, *275*, 18830–18835.
- (13) Boal, A. K.; Cotruvo, J. A., Jr.; Stubbe, J.; Rosenzweig, A. C. Structural basis for activation of class Ib ribonucleotide reductase. *Science* **2010**, *329*, 1526–1530.
- (14) Miller, A.-F. Superoxide dismutases: active sites that save, but a protein that kills. *Curr. Opin. Chem. Biol.* **2004**, *8*, 162–168.
- (15) Wu, J.; Penner-Hahn, J. E.; Pecoraro, V. L. Structural, spectroscopic, and reactivity models for the manganese catalases. *Chem. Rev.* **2004**, *104*, 903–938.
- (16) Umena, Y.; Kawakami, K.; Shen, J.-R.; Kamiya, N. Crystal structure of oxygen-evolving photosystem II at a resolution of 1.9 Å. *Nature* **2011**, *473*, 55–60.
- (17) (a) Mullins, C. S.; Pecoraro, V. L. Reflections on small molecule manganese models that seek to mimic photosynthetic water oxidation chemistry. *Coord. Chem. Rev.* **2008**, *252*, 416–443. (b) Pecoraro, V. L.; Baldwin, M. J.; Gelasco, A. Interaction of manganese with dioxygen and its reduced derivatives. *Chem. Rev.* **1994**, *94*, 807–826. (c) Signorella, S.; Hureau, C. Bioinspired functional mimics of the manganese catalases. *Coord. Chem. Rev.* **2012**, *256*, 1229–1245.
- (18) (a) Wu, A. J.; Penner-Hahn, J. E.; Pecoraro, V. L. Structural, spectroscopic, and reactivity models for the manganese catalases. *Chem. Rev.* **2004**, *104*, 903–938. (b) Young, K. J.; Brennan, B. J.; Tagore, R.; Brudvig, G. W. Photosynthetic water oxidation: insights from manganese model chemistry. *Acc. Chem. Res.* **2015**, *48*, 567–574. (c) Gupta, R.; Taguchi, T.; Lassalle-Kaiser, B.; Bominaar, E. L.; Yano, J.; Hendrich, M. P.; Borovik, A. S. High-spin Mn-oxo complexes and their relevance to the oxygen-evolving complex within photosystem II. *Proc. Natl. Acad. Sci. U. S. A.* **2015**, *112*, 5319–5324. (d) Shook, R. L.; Peterson, S. M.; Greaves, J.; Moore, C.; Rheingold, A. L.; Borovik, A. S. Catalytic reduction of dioxygen to water with a monomeric manganese complex at room temperature. *J. Am. Chem. Soc.* **2011**, *133*, 5810–5817. (e) Triller, M. U.; Pursche, D.; Hsieh, W.-Y.; Pecoraro, V. L.; Rompel, A.; Krebs, B. Catalytic Oxidation of 3,5-Di-tert-butylcatechol by a Series of Mononuclear Manganese Complexes: Synthesis, Structure, and Kinetic Investigation. *Inorg. Chem.* **2003**, *42*, 6274–6283.
- (19) Abbreviations used: 3,5-di-tert-butylcatechol (DBC); 3,5-di-tert-butylsemiquinone (HDBSQ); 3,5-di-tert-butyl-o-benzoquinone (DBQ); 3,5-di-tert-butyl-3-methoxy-6-oxocyclohexa-1,4-dienolate (BMOD)⁻.
- (20) Perrin, D. D.; Armarego, W. L. F.; Perrin, D. R. *Purification of Laboratory Chemicals*, 2nd ed.; Pergamon: Oxford, U.K., 1980.
- (21) (a) Tshuva, E. Y.; Gendziuk, N.; Kol, M. Single-step synthesis of salans and substituted salans by Mannich condensation. *Tetrahedron Lett.* **2001**, *42*, 6405–6407. (b) Tshuva, E. Y.; Goldberg, I.; Kol, M.; Goldschmidt, Z. Zirconium complexes of amine-bis (phenolate) ligands as catalysts for 1-hexene polymerization: peripheral structural parameters strongly affect reactivity. *Organometallics* **2001**, *20*, 3017–3028.
- (22) Robinson, W. R. Perchlorate salts of metal ion complexes: Potential explosives. *J. Chem. Educ.* **1985**, *62*, 1001.
- (23) (a) Berreau, L. M.; Mahapatra, S.; Halfen, J. A.; Houser, R. P.; Young, V. G., Jr.; Tolman, W. B. Reactivity of peroxo- and bis (μ -oxo) dicopper complexes with catechols. *Angew. Chem., Int. Ed.* **1999**, *38*, 207–210. (b) Mahadevan, V.; DuBois, J. L.; Hedman, B.; Hodgson, K. O.; Stack, T. D. P. Exogenous Substrate Reactivity with a [Cu(III)₂O₂]²⁺ Core: Structural Implications. *J. Am. Chem. Soc.* **1999**, *121*, 5583–5584.
- (24) Guha, A.; Chattopadhyay, T.; Paul, N. D.; Mukherjee, M.; Goswami, S.; Mondal, T. K.; Zangrando, E.; Das, D. Radical pathway in catecholase activity with zinc-based model complexes of compartmental ligands. *Inorg. Chem.* **2012**, *51*, 8750–8759.
- (25) Neves, A.; Rossi, L. M.; Bortoluzzi, A. J.; Szpoganicz, B.; Wiezbicki, C.; Schwingel, E.; Haase, W.; Ostrovsky, S. Catecholase activity of a series of dicopper (II) complexes with variable Cu-OH (phenol) moieties. *Inorg. Chem.* **2002**, *41*, 1788–1794.
- (26) Frisch, M. J.; et al. *Gaussian 03*; Gaussian, Inc.: Wallingford, CT, 2004.
- (27) Lovell, T.; Himo, F.; Han, W.-G.; Noodleman, L. Density functional methods applied to metalloenzymes. *Coord. Chem. Rev.* **2003**, *238–239*, 211–232.
- (28) Becke, A. D. Density-functional exchange-energy approximation with correct asymptotic behavior. *Phys. Rev. A: At., Mol., Opt. Phys.* **1988**, *38*, 3098–3100.

- (29) Perdew, J. P. Density-functional approximation for the correlation energy of the inhomogeneous electron gas. *Phys. Rev. B: Condens. Matter Mater. Phys.* **1986**, *33*, 8822–8824.
- (30) SADABS, version 2.03; Bruker AXS Inc.: Madison, WI, 2002.
- (31) Sheldrick, G. M. Phase annealing in SHELX-90: direct methods for larger structures. *Acta Crystallogr., Sect. A: Found. Crystallogr.* **1990**, *46*, 467–473.
- (32) Sheldrick, G. M. *SHELXL-2013*; University of Gottingen: Gottingen, Germany, 2013.
- (33) SAINT, version 6.02; Bruker AXS Inc.: Madison, WI, 2002.
- (34) *Diamond, Visual Crystal Structure Information System*, version 3.1; Crystal Impact: Bonn, Germany, 2004.
- (35) In order to determine the stoichiometries of these reactions, we allowed the μ -OMe compounds **7** and **8** as well as the powdery solid obtained with the ligand $H_2L^{t-Bu,F-Bu}$ to react with H_2DBC at various molecular proportions. In all cases, yields are almost equal when two or more molecular equivalents of H_2DBC is used per equivalent of the binuclear μ -hydroxido intermediates. The overall yield is, however, half as much when the reactants are taken in 1:1 mol equiv.
- (36) Vlcek, A., Jr. Metal and Ligand Oxidation States in Dioxolene Complexes: Meaning, Assignment and Control. *Comments Inorg. Chem.* **1994**, *16*, 207–228.
- (37) (a) Mandal, D.; Chatterjee, P. B.; Bhattacharya, S.; Choi, K.-Y.; Clérac, R.; Chaudhury, M. Tetra-, tri-, and mononuclear manganese(II/III) complexes of a phenol-based N_2O_2 capping ligand: use of carboxylates as ancillary ligands in tuning the nuclearity of the complexes. *Inorg. Chem.* **2009**, *48*, 1826–1835. (b) Coggins, M. K.; Martin-Diaconescu, V.; DeBeer, S.; Kovacs, J. A. Correlation between structural, spectroscopic, and reactivity properties within a series of structurally analogous metastable manganese(III)–alkylperoxo complexes. *J. Am. Chem. Soc.* **2013**, *135*, 4260–4272. (c) Attia, A. S.; Pierpont, C. G. Valence tautomerism within a linear polymer consisting of pyrazine-bridged manganese–quinone subunits. synthesis and characterization of $[Mn^{III}(\mu-pyz)(3,6-DBSQ)(3,6-DBCat)]_n$. *Inorg. Chem.* **1997**, *36*, 6184–6187.
- (38) (a) Cass, M. E.; Gordon, N. R.; Pierpont, C. G. Catecholate and semiquinone complexes of vanadium. Factors that direct charge distribution in metal-quinone complexes. *Inorg. Chem.* **1986**, *25*, 3962–3967. (b) Chang, H.-C.; Kitagawa, S. An Unprecedented mixed-charged state in a supramolecular assembly of ligand-based mixed-Valence redox isomers $(ET^+)_3[Cr^{III}(Cl_4SQ)_2(Cl_4Cat)]^- [Cr^{III}(Cl_4SQ)(Cl_4Cat)_2]^{2-}$. *Angew. Chem., Int. Ed.* **2002**, *41*, 130–133.
- (39) (a) Arzberger, S.; Soper, J.; Anderson, O. P.; la Cour, A.; Wicholas, M. Synthesis and structure of an air-stable, free-radical cobalt (III) semiquinone complex. *Inorg. Chem.* **1999**, *38*, 757–761. (b) Lange, C. W.; Conklin, B. J.; Pierpont, C. G. Radical superexchange in semiquinone complexes containing diamagnetic metal ions. 3,6-Di-tert-butyl-1,2-semiquinone complexes of zinc(II), cobalt(III), gallium(III), and aluminum(III). *Inorg. Chem.* **1994**, *33*, 1276–1283.
- (40) (a) Kabanos, T. A.; White, A. P. J.; Williams, D. J.; Woollins, J. D. Synthesis and X-ray structures of bis(3,5-di-tert-butylcatecholato)-(phenanthroline)-vanadium(IV) and its vanadium(V) analogue $[V(dtbc)_2(phen)][SbF_6]$. *J. Chem. Soc., Chem. Commun.* **1992**, 17–18. (b) Kabanos, T. A.; Slawin, A. M. Z.; Williams, D. J.; Woollins, J. D. The preparation and X-ray structure of $V(N_3S_2)(dtbc)(phen)\cdot CHCl_3$ (dtbc = di-tert-butylcatecholate, phen = phenanthroline). *J. Chem. Soc., Chem. Commun.* **1990**, 193–194.
- (41) We failed to refine the crystal structure of compound **1** at room temperature in spite of our repeated attempts because of the high degree of disorder shown by the tert-butyl groups of the associated ligands.
- (42) Kessel, S. L.; Emberson, R. M.; Debrunner, P. G.; Hendrickson, D. N. Iron(III), manganese(III), and cobalt(III) complexes with single chelating o-semiquinone ligands. *Inorg. Chem.* **1980**, *19*, 1170–1178.
- (43) (a) Hitomi, Y.; Ando, A.; Matsui, H.; Ito, T.; Tanaka, T.; Ogo, S.; Funabiki, T. Aerobic catechol oxidation catalyzed by a bis(μ -oxo)dimanganese(III, III) complex via a manganese(II)–semiquinonate complex. *Inorg. Chem.* **2005**, *44*, 3473–3478. (b) Benelli, C.; Dei, A.; Gatteschi, D.; Pardi, L. Electronic and CD spectra of catecholate and semiquinonate adducts of zinc(II) and nickel(II) tetraazamacrocyclic complexes. *Inorg. Chem.* **1989**, *28*, 1476–1480.
- (44) (a) Neves, A.; Erthal, S. M. D.; Vencato, I.; Ceccato, A. S.; Mascarenhas, Y. P.; Nascimento, O. R.; Horner, M.; Batista, A. A. Synthesis, crystal structure, electrochemical, and spectroelectrochemical properties of the new manganese(III) complex $[Mn^{III}(BBPEN)]\cdot [PF_6]$ [$H_2BBPEN = N,N'$ -bis(2-hydroxybenzyl)- N,N' -bis(2-methylpyridyl)ethylenediamine]. *Inorg. Chem.* **1992**, *31*, 4749–4755. (b) Li, X.; Pecoraro, V. L. Stepwise, metal-assisted decarboxylation promoted by manganese: reactivity relationship between manganese and vanadium. *Inorg. Chem.* **1989**, *28*, 3403–3410.
- (45) (a) Andrews, L.; Prochaska, E. S.; Loewenschuss, A. Resonance Raman and Ultraviolet Absorption Spectra of the Triiodide Ion Produced by Alkali Iodide-Iodine Argon Matrix Reactions. *Inorg. Chem.* **1980**, *19*, 463–465. (b) Gabes, W.; Stufkens, D. J. Electronic absorption spectra of symmetrical and asymmetrical trihalide ions. *Spectrochim. Acta, Part A* **1974**, *30*, 1835–1841.
- (46) (a) Abdel-Mohsen, H. T.; Conrad, J.; Beifuss, U. Laccase-catalyzed synthesis of catechol thioethers by reaction of catechols with thiols using air as an oxidant. *Green Chem.* **2014**, *16*, 90–95. (b) Hahn, V.; Davids, T.; Lalk, M.; Schauer, F.; Mikolasch, A. Enzymatic cyclizations using laccases: Multiple bond formation between dihydroxybenzoic acid derivatives and aromatic amines. *Green Chem.* **2010**, *12*, 879–887.
- (47) Schnepf, R.; Sokolowski, A.; Müller, J.; Bachler, V.; Wiegardt, K.; Hildebrandt, P. Resonance Raman spectroscopic study of phenoxyl radical complexes. *J. Am. Chem. Soc.* **1998**, *120*, 2352–2364.
- (48) Sokolowski, A.; Bothe, E.; Bill, E.; Weyhermüller, T.; Wiegardt, K. Phenoxyl radical complexes of chromium(III). *Chem. Commun.* **1996**, 1671–1672.
- (49) Sokolowski, A.; Müller, J.; Weyhermüller, T.; Schnepf, R.; Hildebrandt, P.; Hildenbrand, K.; Bothe, E.; Wiegardt, K. Phenoxyl radical complexes of zinc(II). *J. Am. Chem. Soc.* **1997**, *119*, 8889–8900.
- (50) (a) Attia, A. S.; Pierpont, C. G. New semiquinone/catecholate complexes that exhibit valence tautomerism. Synthesis and characterization of $Mn^{III}(thf)_2(3,6-DBSQ)(3,6-DBCat)$ and observations on the $Mn^{IV}(3,6-DBSQ)_2(3,6-DBCat)/Mn^{III}(3,6-DBSQ)_3$ equilibrium in the solid state. *Inorg. Chem.* **1998**, *37*, 3051–3056. (b) Attia, A. S.; Pierpont, C. G. Valence Tautomerism for quinone complexes of manganese: members of the $Mn^{IV}(N-N)(Cat)_2\cdot Mn^{III}(N-N)(SQ)(Cat)\cdot Mn^{II}(N-N)(SQ)_2$ series. *Inorg. Chem.* **1995**, *34*, 1172–1179. (c) Komatsuzaki, H.; Shiota, A.; Hazawa, S.; Itoh, M.; Miyamura, N.; Miki, N.; Takano, Y.; Nakazawa, J.; Inagaki, A.; Akita, M.; Hikichi, S. Manganese(II) semiquinonate and manganese(III) catecholato complexes with tridentate ligand: modeling the substrate-binding state of manganese-dependent catechol dioxygenase and reactivity with molecular oxygen. *Chem. - Asian J.* **2013**, *8*, 1115–1119.